Published in final edited form as:

Nature. 2015 November 26; 527(7579): 539–543. doi:10.1038/nature15519.

Endoperoxide formation by an α-ketoglutarate-dependent mononuclear non-haem iron enzyme

Wupeng Yan[#1], **Heng Song**[#2], **Fuhang Song**[3], **Yisong Guo**[6], **Cheng-Hsuan Wu**[2], **Ampon Sae Her**[2], **Yi Pu**[2,4], **Shu Wang**[2], **Nathchar Naowarojna**[2], **Andrew Weitz**[6], **Michael P. Hendrich**[6], **Catherine E. Costello**[2,4], **Lixin Zhang**[3], **Pinghua Liu**[2], and **Yan Jessie Zhang**[1,5]

[1]Department of Molecular Biosciences, University of Texas at Austin, Austin, Texas 78712, USA.

[2]Department of Chemistry, Boston University, Boston, Massachusetts 02215, USA.

[3]CAS Key Laboratory of Pathogenic Microbiology and Immunology, Institute of Microbiology, Chinese Academy of Sciences, Beijing 100101, China.

[4]Center for Biomedical Mass Spectrometry, Boston University School of Medicine, Boston, Massachusetts 02118, USA.

[5]Institute for Cellular and Molecular Biology, University of Texas at Austin, Austin, Texas 78712, USA.

[6]Department of Chemistry, Carnegie Mellon University, 4400 Fifth Avenue, Pittsburgh, Pennsylvania 15213, USA.

[#] These authors contributed equally to this work.

Abstract

Many peroxy-containing secondary metabolites[1,2] have been isolated and shown to provide beneficial effects to human health[3–5]. Yet, the mechanisms of most endoperoxide biosyntheses are not well understood. Although endoperoxides have been suggested as key reaction intermediates in several cases[6–8], the only well-characterized endoperoxide biosynthetic enzyme is prostaglandin H synthase, a haem-containing enzyme[9]. Fumitremorgin B endoperoxidase (FtmOx1) from *Aspergillus fumigatus* is the first reported α-ketoglutarate-dependent mononuclear non-haem iron enzyme that can catalyse an endoperoxide formation reaction[10–12]. To elucidate the mechanistic details for this unique chemical transformation, we report the X-ray crystal structures

Correspondence and requests for materials should be addressed to P.L. (pinghua@bu.edu) or Y.J.Z. (jzhang@cm.utexas.edu) or L.Z. (lzhang03@gmail.com)..

Author Contributions P.L., Y.J.Z. and L.Z. designed the study. W.Y. conducted the crystallization experiments and structure determination. H.S., F.S., A.S.H., S.W. and N. N. conducted the biochemical studies. C.-H.W., Y.P. and C.E.C. performed the MS–MS analyses. H.S., Y.G., M.P.H. and A.W. conducted the pre-steady state kinetics and EPR characterization. The manuscript was written by P.L., Y.J.Z. and L.Z. with input from all contributing authors.

Author Information The structural factors and coordinates of FtmOx1 and its complexes with either α -KG or fumitremorgin B have been deposited in the Protein Data Bank with accession codes 4Y5T, 4Y5S and 4ZON. The authors declare no competing financial interests. Readers are welcome to comment on the online version of the paper.

Online Content Methods, along with any additional Extended Data display items and Source Data, are available in the online version of the paper; references unique to these sections appear only in the online paper.

Supplementary Information is available in the online version of the paper.

of FtmOx1 and the binary complexes it forms with either the co-substrate (α-ketoglutarate) or the substrate (fumitremorgin B). Uniquely, after α-ketoglutarate binding to the mononuclear iron centre in a bidentate fashion, the remaining open site for oxygen binding and activation is shielded from the substrate or the solvent by a tyrosine residue (Y224). Upon replacing Y224 with alanine or phenylalanine, the FtmOx1 catalysis diverts from endoperoxide formation to the more commonly observed hydroxylation. Subsequent characterizations by a combination of stopped-flow optical absorption spectroscopy and freeze-quench electron paramagnetic resonance spectroscopy support the presence of transient radical species in FtmOx1 catalysis. Our results help to unravel the novel mechanism for this endoperoxide formation reaction.

The verruculogen biosynthetic gene cluster was identified through bioinformatic analysis[10], and its chemical scaffold is assembled by a non-ribosomal peptide synthetase, followed by several tailoring reactions. Among them, the FtmOx1-catalysed endoperoxide formation reaction is the most notable (Fig. 1a). Recent biochemical characterizations indicate that, unlike prostaglandin H synthase, FtmOx1 is an α -ketoglutarate (α -KG)-dependent mononuclear non-haem iron enzyme[11,12]. Further characterization indicates that molecular oxygen (O_2) is incorporated into verruculogen without the O–O bond scission[11,12], distinguishing FtmOx1 from all currently known α -KG-dependent mononuclear non-haem iron enzymes[13–17].

To unravel the mechanistic details of FtmOx1 catalysis, we first characterized the FtmOx1–α -KG complex using anaerobically purified and Fe^{2+}-reconstituted FtmOx1 (FtmOx1-Fe^{II}). Upon mixing the reconstituted enzyme with α -KG under anaerobic conditions, a pink species appeared (pink trace, extinction coefficient ε_{520} of ~ 166 M^{-1} cm^{-1}, Fig. 1b). The dissociation constant (K_d) of this species was ~ 185 ± 35 μ M (Extended Data Fig. 1a), close to the K_d values of Fe^{II}–α -KG complexes of other mononuclear non-haem iron enzymes (for example, that of TauD)[18]. Upon exposure to O_2 and in the absence of the substrate fumitremorgin B (**1**), the pink species faded and a blue chromophore with a λ_{max} at ~ 600 nm developed within 30 min (blue trace, Fig. 1b). Tandem mass spectrometry (MS/MS) analysis of the blue species indicated the oxidation of Y224 to dihydroxyphenylalanine (DOPA, Fig. 1c), which is the result of a self-hydroxylation reaction as observed in other mononuclear non-haem iron enzymes[19]. Notably, the presence of the substrate fumitremorgin B (**1**) prevented the FtmOx1 self-hydroxylation reaction (Extended Data Fig. 2). All of these properties are consistent with the formation of the FtmOx1-Fe^{II}–α -KG complex.

In previous studies, ascorbate was included as an additional reductant[11,12], although its role in FtmOx1 catalysis was not known[11,12]. We observed that FtmOx1 is capable of catalysing fumitremorgin B (**1**) oxidation in the absence of ascorbate (Fig. 1d and Extended Data Fig. 3). At a fixed FtmOx1-Fe^{II}:fumitremorgin B ratio of 1:1.5 and with an excess of O_2, the amount of product increased with the amount of α -KG until the α -KG:FtmOx1-Fe^{II} ratio reached 1.0 (Fig. 1e and Extended Data Fig. 4). In contrast, when the O_2:FtmOx1-Fe^{II} ratio was below 1.0, only a small amount (~0.2 equivalent) of product was formed. Above 1.0, the amount of product increased with the increasing amount of O_2, and plateaued when the O_2:FtmOx1-Fe^{II} ratio was > 2.0 (Fig. 1f and Extended Data Fig. 4). These results strongly

suggest that each FtmOx1-catalysed turnover consumes one equivalent of α -KG and two equivalents of O_2. Unexpectedly, under our assay conditions, compound **3** rather than verruculogen (**2**) was the dominant product (Fig. 1e, f and Supplementary Information).

We determined the FtmOx1 crystal structure at 1.95 Å resolution with the phase derived from selenomethionine-labelled FtmOx1 using the single-wavelength anomalous dispersion method. FtmOx1 folds as a 'jelly roll', a prevalent fold in mononuclear non-haem iron enzymes (Fig. 2a)[13]. Two molecules in each asymmetric unit form a functional dimer, consistent with our size-exclusion chromatography profile and previous literature reports[11,12]. The dimer interface (2,461.6 $Å^2$) accounts for 17.1% of the FtmOx1 surface. The active site pocket at the dimer interface has a volume of 222.6 $Å^3$, as calculated by the DogSite Server[20]. This spacious pocket is partitioned into two parts: a hydrophilic region where the non-haem iron centre is located and a hydrophobic pocket formed by L64, F115, and F233 from one monomer with I267 and V268 from the other (Fig. 2b).

H129, H205, D131, and three well-ordered water molecules form an approximate octahedral coordination to the mononuclear iron (Fig. 2c). One of the water ligands is hydrogen-bonded to Y224, whose proximity to the mononuclear iron centre (~ 4.4 Å) explains the formation of DOPA in the FtmOx1 self-hydroxylation reaction (Fig. 1c). Co-crystallization or soaking of the co-substrate α -KG led to an identical FtmOx1-Fe^{ii}–α -KG complex, in which α -KG binds to the iron centre in a bidentate fashion by replacing two water molecules (Fig. 2d). In the FtmOx1-Fe^{II}–α -KG complex, the 2-keto group of α -KG coordinates to the iron centre *trans* to D131. Its 1-carboxylate group binds *trans* to H205, which is the distal histidine of the 2-His-1-carboxylate facial triad (Fig. 2d and Extended Data Fig. 5a)[13]. In this FtmOx1-Fe^{II}–α -KG complex, the remaining water ligand (a potential site for O_2 binding and activation) is completely shielded from solvent or substrate by Y224 (Fig. 2d and Supplementary Video 1). In contrast, in most reported structures of enzyme–α -KG complexes, the 1-carboxylate of α -KG coordinates *trans* to the proximal histidine of the facial triad motif[13], and the remaining open site for O_2 binding and activation directly points towards the substrate. As a result, the oxoferryl (Fe^{IV}=O) species produced from oxygen activation is accessible to the substrate for oxidative transformations (for example, TauD in Fig. 2e and Supplementary Video 2)[21].

To examine whether Y224 changes location upon substrate binding, we also solved the structure of the FtmOx1-Fe^{II}–fumitremorgin B complex at a resolution of 2.2 Å (Fig. 2f). The location of the positive density is consistent for all data sets collected for this complex by either co-crystallization or soaking (>15 data sets). Substrate is modelled into the density at the active site with an average occupancy of ~60% owing to the high hydrophobicity of fumitremorgin B (Extended Data Fig. 5b). In this complex, Y224 adopts an identical conformation to that observed in the FtmOx1 alone (Fig. 2c) and FtmOx1-Fe^{II}–α -KG complexes (Fig. 2d). Rings A and B of the substrate form π –π stacking with the Y224 side chain at a distance of ~ 3.3 Å (Fig. 2f). Superimposition of the structures of the FtmOx1-Fe^{II}–α -KG complex onto the FtmOx1-Fe^{II}–fumitremorgin B complex revealed that the side chain of Y224 effectively separates the potential O_2 binding site from the substrate binding pocket (Fig. 2g, Extended Data Fig. 5c and Supplementary Video 1). This is in notable

contrast to TauD, in which the oxygen binding and activation site directly faces the substrate (Extended Data Fig. 5d and Supplementary Video 2)[21].

On the basis of the strategic positioning of Y224 in the FtmOx1 active site, we next examined the role it plays in FtmOx1 catalysis. We characterized two Y224 variants, Y224A- and Y224F-substituted FtmOx1. The enzyme–α -KG complexes of both variants exhibit K_d values close to that of the wild-type FtmOx1 (Extended Data Fig. 1b, c). However, the product profiles of both variants were very different (Fig. 3). The Y224A-substituted variant produced a mixture of at least five detectable products with mainly dealkylation products (compounds **4 5** and **6**). Endoperoxides (**2** and **3**) only account for ~15% of the product population (Fig. 3a, b).

The Y224F-substituted variant also produced endoperoxides (**2** and **3**) and dealkylation products (**4** and **5**). In addition, there were more endoperoxides (**2** and **3**) formed by the FtmOx1(Y224F) variant relative to the FtmOx1(Y224A) variant (~ 35% versus ~ 15% of the product mixture, Fig. 3a). For the FtmOx1(Y224F)-Fe^{II}–α -KG complex in the absence of the substrate fumitremorgin B (**1**), exposure to O_2 caused the complex to slowly change colour to blue, which implies DOPA formation (Extended Data Fig. 6a). DOPA formation can be explained by two sequential hydroxylation steps (F224→ Y224 and Y224→ DOPA224). Indeed, this conclusion was supported by MS/MS analysis of this variant (Extended Data Fig. 6b–e). Thus, the higher level of endoperoxides (**2** and **3**) produced by the FtmOx1(Y224F) variant is probably attributed to the conversion of the variant to wild-type FtmOx1, which provides further evidence supporting the key role of Y224 in FtmOx1 catalysis.

Mononuclear non-haem iron enzymes catalyse a wide range of reactions[13–17]. Recently, unique transformations have been reported which demonstrate the functional versatility of this class of enzymes, including oxidative dehydrogenation in epoxide formation[22], chlorination[23,24], epimerization[25,26], and C–C bond cleavage[27]. FtmOx1 provides a further example of this diversity[11,12]. On the basis of our structural and biochemical information, we propose a preliminary FtmOx1 mechanistic model (Fig. 4). After α -KG and substrate binding, the first molecule of O_2 is activated to produce an Fe^{IV}=O species (species **B**) by a mechanism similar to that of other members of this class of enzymes[28]. Uniquely, in FtmOx1, because the O_2 activation site is shielded from the substrate by Y224, direct oxidation of the substrate by the Fe^{IV} =O species is less likely. Instead, the Fe^{IV}=O species oxidizes Y224 to a tyrosyl radical (species **C**), which then removes a hydrogen atom from the fumitremorgin B C21 position to form a substrate-based radical (species **D**). A second molecule of O_2 reacts with species **D** to form a peroxyl radical (species **E**). It then reacts with the other prenyl arm to produce the endoperoxide along with the formation of a carbon centre radical at the C26 position (species **F**). Species **F** can re-oxidize Y224 to a tyrosyl radical (species **G**). Starting from species **G**, two pathways are possible. FtmOx1 can follow a mechanism similar to prostaglandin synthase H (ref. 9) in which once the tyrosyl radical is formed, multiple cycles of endoperoxide formation can be mediated through this radical (pathway I, Fig. 4). However, the production of compound **3** in the FtmOx1 reaction points to another possibility (pathway II, Fig. 4), in which the two electrons provided by the **2**→ **3**

oxidation process reduce both Fe^{3+} and the tyrosyl radical to the resting state of FtmOx1 (species **A**).

The formation of a small amount of endoperoxides in Y224A- and Y224F-substituted FtmOx1 may be due to two competing pathways: the hydroxyl-rebound and the endoperoxide formation pathways (Extended Data Fig. 7). After Fe^{IV}=O is formed, it may directly remove a hydrogen atom from the fumitremorgin B (**1**) C21 position to form a substrate-based radical (species **C′,** Extended Data Fig. 7). Subsequent rebound by the hydroxyl radical will lead to the formation of hydroxylation products (pathway I′ , Extended Data Fig. 7). Decomposition of the hydroxylation reaction product forms compounds **4** and **5**. At the same time, the substrate-based radical (species **C′**) may be trapped by a second molecule of O_2, which leads to endoperoxide formation (pathway II′, Extended Data Fig. 7).

To gain evidence supporting the presence of radical species in FtmOx1 catalysis as outlined in our FtmOx1 mechanistic model (Fig. 4), we conducted spin-trapping experiments using 5,5-dimethyl-1-pyrroline *n*-oxide (DMPO) as the reagent. In the presence of 50 equivalents of DMPO, further oxidation of verruculogen **2** to **3** was markedly suppressed, and **2** was the dominant product (Fig. 5a). This result provides evidence supporting the involvement of radicals in FtmOx1 catalysis. Next, the FtmOx1 reaction was monitored with stopped-flow optical absorption spectroscopy (Fig. 5b). The UV–visible spectrum of the solution generated after rapid mixing of O_2-saturated buffer with the FtmOx1-Fe^{II}–fumitremorgin B–α -KG complex demonstrated the accumulation of a transient species centred at ~420 nm. The amount of this species maximized at ~ 0.2 s and then decayed within ~3 s. This wavelength differs from the tyrosyl radicals observed in ribonucleotide reductase[29] and another reported α -KG-dependent iron enzyme, CarC[26] (a peak at 410 nm with a shoulder at 390 nm). Chemical quench experiments performed under the same conditions indicated that the consumption of substrate **1** and the formation of products (**2** and **3**) occurred on the timescale of seconds per cycle (Extended Data Fig. 8a), suggesting that the 420 nm species observed in the stopped-flow optical absorption spectroscopy experiments is a kinetically competent intermediate. FtmOx1 catalysis was then investigated by rapid freeze-quench in conjunction with electron paramagnetic resonance (EPR) spectroscopy. Two EPR signals were observed at 0.01 s (earliest possible time on instrument) and were highest at ~ 0.2 s after the rapid mixing of O_2-saturated buffer with the FtmOx1-Fe^{II}–fumitremorgin B–α -KG complex (Extended Data Fig. 9a). The first EPR signal with resonances at g = 4.54, 4.26, and 3.93 (Extended Data Fig. 9b) belongs to a high-spin Fe^{3+} species having axial and rhombic zero-field splitting parameters of $|D| < 0.5$ cm^{-1} and $E/D \sim 0.26$, respectively. These parameters are not typical of adventitious Fe^{3+}. The second EPR signal was in the g = 2 region and most likely belongs to a radical species (Fig. 5c and Extended Data Fig. 9c). The formation and decay of this radical signal closely followed the kinetics of the 420 nm absorption feature observed in stopped-flow optical absorption spectroscopy experiments (Extended Data Fig. 8b), indicating that they are from the same intermediate species. Spin quantification of the EPR signals at ~0.2 s revealed that the Fe^{3+} and radical species accumulated to ~0.35 and ~0.25 equivalents, respectively. The width of the radical EPR signal (~12 mT edge-to-edge width, Fig. 5c) was significantly broader than that of magnetically isolated organic or protein radical signals[29]. Such broadening could be due to a

magnetic dipolar interaction of the radical species with an adjacent spin centre, most likely the Fe^{3+} centre depicted in species **D**, **E**, or **F** in Fig. 4.

In summary, our FtmOx1 structural and biochemical characterization provides a notable example of the catalytic versatility of mononuclear non-haem iron enzymes and how changes in the secondary coordination sphere to the non-haem iron facilitate unprecedented chemical transformations.

METHODS

No statistical methods were used to predetermine sample size.

Materials and experimental procedures

Fumitremorgin B was isolated from *Aspergillus fumigatus* strain IM-MF330 according to the procedure summarized in a later section. All reagents were purchased from Sigma-Aldrich unless otherwise stated.

Nuclear magnetic resonance (NMR) spectra were obtained on a Bruker Avance DRX600 spectrometer in the solvents indicated and referenced to residual ^{1}H and ^{13}C signals in deuterated solvents. High-resolution electrospray ionization (ESI) mass spectroscopy (MS) measurements were obtained on a Bruker micrOTOF mass spectrometer. High-performance liquid chromatography (HPLC) was performed using an Agilent 1200 Series separations module equipped with Agilent 1200 Series diode array detectors and an Agilent 1200 Series fraction collector, controlled using ChemStation. UV–vis analysis was performed on a Varian Cary 100 Bio UV–vis spectrophotometer.

Sub-cloning and overexpression of wild-type, Y224F- and Y224A-substituted FtmOx1

The coding sequence of the *FtmOx1* gene from *A. fumigatus* Af293 (accession number: XM_742088) was sub-cloned into the EcoRI and XhoI restriction sites of the pASK-IBA3^{+} vector, which places it under the control of the *tet*-promoter and allows for the production of C-terminally strep-tagged FtmOx1. The final recombinant FtmOx1 includes some extra amino acid residues at the N terminus and a Strep-tag at the C terminus for purification. The residue numbering used in this manuscript is based on the FtmOx1 sequence deposited in GenBank (accession number: XM_742088). Y224F- and Y224A-substituted FtmOx1 were generated using a Stratagene QuikChange II kit according to the manufacturer's instructions.

Plasmids encoding wild-type, Y224F-, and Y224A-substituted FtmOx1 mutant genes were used to transform *Escherichia coli* BL21 (DE3) cells (Invitrogen Inc.) for protein overexpression. A single colony was used to inoculate a starter culture, which was incubated at 37 °C overnight. Production cultures were grown at 37 °C in Luria–Bertani medium supplemented with 100 μ g ml^{-1} ampicillin to an optical density (OD_{600}) of ~0.8 and then cooled to 25 °C. The FtmOx1 protein production was induced by the addition of anhydrotetracycline to a final concentration of 250 μ g l^{-1}. The cultures were grown at 25 °C for an additional 16 h before harvesting.

Purification was performed at 4 °C. In a typical purification, ~30 g wet cell paste was resuspended in 100 ml of anaerobic buffer (100 mM Tris-HCl, 50 mM NaCl, and 5 mM 1,10-phenanthroline (pH 7.5)) in an anaerobic Coy chamber. Lysozyme (1.0 mg ml^{-1} final concentration) and DNase I (100 U per gram of cell) were then added into the cell suspension, and the mixture was incubated on ice for 40 min with gentle agitation. The cells were disrupted by sonication (20 cycles of 10 s bursts) using a Fisher Scientific Model 505 Sonic Dismembrator. The supernatant and the cell debris were anaerobically separated by centrifugation at 4 °C for 30 min at 20,000 *g*. Streptomycin sulfate was added into the supernatant (~ 100 ml) to a final concentration of 1% (w/v), and the mixture was incubated on ice for 30 min with gentle agitation. The DNA precipitate was then removed by centrifugation at 20,000 *g* for 40 min at 4 °C. The resulting supernatant was mixed with Strep-Tactin resin (50 ml) and incubated on ice for 30 min. After the cell lysate was drained by gravity, the column was washed with washing buffer (100 mM Tris-HCl and 150 mM NaCl (pH 7.5)) until the OD_{260} was < 0.05. The FtmOx1 protein was reconstituted by incubating the protein-loaded resin with 50 ml of a solution containing 3.0 mM ammonium ferrous sulfate and 5.0 mM ascorbate at 4 °C for 10 min. After the excess solution was drained by gravity, the resin was further washed with washing buffer until the OD_{280} was < 0.05. Recombinant FtmOx1 was eluted with elution buffer (2.5 mM desthiobiotin in 100 mM Tris-HCl and 50 mM NaCl (pH 7.5)). The eluted protein was concentrated, flash frozen with liquid nitrogen, and stored at − 80 °C. From 30 g of wet cell paste, ~400 mg of protein was obtained. The purity of the protein was shown by SDS–PAGE (12%) as a single band. The FtmOx1 concentration was calculated using ε_{280} nm of 43,288 M^{-1} cm^{-1} determined by amino acid analysis.

Selenomethionine-incorporated FtmOx1 was prepared using a modified medium. A single colony was used to inoculate 50 ml Luria–Bertani medium supplemented with 100 μ g ml^{-1} ampicillin, which was incubated at 37 °C until the OD_{600} was ~0.5. The pre-culture (2 ml) was transferred into 150 ml of minimal media (1 liter minimal media contained 50 ml glycerol, 12.8 g Na_2HPO_4–$7H_2O$, 3 g KH_2PO_4, 0.5 g NaCl, 1 g NH_4Cl, 0.2% glucose, 0.1 mM $CaCl_2$, and 2.0 mM $MgSO_4$) supplemented with 100 μ g ml^{-1} ampicillin, which was incubated at 37 °C for an additional 5 h. Then, 10 ml of the pre-culture was transferred into 1 liter minimal media supplemented with 100 μ g ml^{-1} ampicillin and incubated at 37 °C for 12 h. Subsequently, 10 ml 100× amino acid solution mix (100× amino acid solution contained 100 mg lysine, 100 mg threonine, 100 mg phenylalanine, 50 mg leucine, 50 mg isoleucine, and 50 mg valine in 10 ml H_2O) and 100× selenomethionine solution (60 mg L-selenomethionine in 10 ml H_2O) were added to the culture medium. After 0.5 h, the temperature was decreased to 25 °C, and FtmOx1 over-expression was induced by the addition of anhydrotetracycline to a final concentration of 250 μ g l^{-1}. The cultures were grown at 18 °C for an additional 12 h before harvesting.

Selenomethionine-incorporated FtmOx1 was purified according to the same procedure described earlier. From 5 g of wet cell paste, ~15 mg of selenomethionine-incorporated FtmOx1 was obtained.

Before crystallization, FtmOx1 was further purified by gel filtration (Superdex 200, GE Healthcare) in buffer containing 100 mM Tris-HCl at pH 7.5 and 50 mM NaCl. After gel

filtration, FtmOx1 was concentrated to ~10 mg ml^{-1} and stored at − 80 °C for future crystallization experiments.

Isolation of fumitremorgin B

Aspergillus fumigatus strain IM-MF330 was isolated from a mud sample collected from the Yellow Sea. A small number of spores growing on a potato dextrose agar slant was inoculated into a 250-ml conical flask containing 40 ml of liquid medium (20% potato infusion, 2.0% glucose, 3.5% sea salt, and distilled water) and then cultured at 28 °C for 3 days on a rotary shaker at 160 rpm. The seed culture (5 ml) was inoculated into 1,000-ml conical flasks, each containing 130 g rice and 80 ml artificial seawater, and incubated without aeration for 19 days. The fermentation product was exhaustively extracted with EtOAc:MeOH (80:20) to yield a crude extract. The crude extract was partitioned between EtOAc and H_2O. The EtOAc layer (10.4 g) was applied to a column of silica gel using a gradient solvent system of 50–100% petroleum ether/CH_2Cl_2 and 0–100% MeOH/CH_2Cl_2 to afford 15 fractions. Fraction MF330F was passed through a Sephadex LH-20 column and eluted with petroleum-ether: CH_2Cl_2:MeOH (5:5:1) to yield 5 sub-fractions. The third fraction MF30F3 was subsequently subjected to HPLC fractionation (Agilent Zorbax SB-C18 5 μ m 250 × 9.4 mm column, 3.0 ml min^{-1}, 65% MeOH) to yield verruculogen and fumitremorgin B, respectively.

Crystallization and data collection

FtmOx1 crystallization was set up using the sitting-drop vapour diffusion method by mixing protein and crystallization buffer (100 mM MES (pH 6.5), 50 mM $CoCl_2$, and 2 M ammonium sulfate) at a ratio of 2:1 at room temperature. Sheet-like crystals were visible after 7 days. The FtmOx1 and α -ketoglutarate (α -KG) complex was obtained using both soaking and co-crystallization methods, which led to identical models. Crystal soaking was conducted by transferring the pre-formed FtmOx1 crystals into crystallization mother liquor containing 1 mM α -KG and incubated for 2 h at room temperature. Co-crystallization trials included pre-mixture of the protein with α -KG at a ratio of 1:100 for 2 h before crystallization setup. The crystals were cryoprotected by the addition of 25% glycerol in mother liquor before being vitrified in liquid nitrogen for data collection. To obtain the structure of the FtmOx1–fumitremorigin B complex, we crystallized FtmOx1 in an anaerobic chamber using identical conditions. Sheet-like crystals appeared within 3 days and continued to grow for another week before reaching maximal size. Fumitremorgin B was dissolved in buffer containing degased crystallization mother liquor with 0.05% TritonX-100 and 20% glycerol to saturation. After centrifugation, to discard insoluble material, the mother liquor containing a saturating amount of fumitremorgin B was used to soak FtmOx1 crystals as sitting drops for 90 min until cryoprotected with degased mother liquor with 30% glycerol.

Crystal diffraction data were collected at the Advanced Photon Source beamline BL23-ID-B (Argonne, Illinois) for FtmOx1 (wavelength 0.97931 Å) and selenomethionine-incorporated FtmOx1 (wavelength 0.97958 Å). The diffraction data for the FtmOx1–α -KG and FtmOx1–fumitremorgin B binary complexes were collected at the Advanced Light Source beamline BL5.0.3 (Berkeley, California) at wavelength 0.97648 Å. All data collection were conducted

within liquid nitrogen stream at 100 K. The data were processed using the program HKL2000[30]. The statistics for data collection are summarized in Extended Data Table 1.

Structure determination and refinement

The FtmOx1 structure was determined by the single anomalous dispersion method using the selenomethionine data set with phase information to 3.5 Å resolution. The positions of the selenium were determined and refined by Phenix.Autosol[31–33] followed by the density modification program DM in CCP4 suite[34–45]. An initial model was built based on the phase information using the Buccaneer program[40,46,47], further extended and corrected manually by the COOT program[48]. The resolution was extended to the high-resolution limit of 1.95 Å using the native protein data set. Iterative cycles of optimization were performed to improve the quality of the model using the refinement program PHENIX.Refine[49–55], followed by manual rebuilding in COOT[48]. A portion of the of diffraction data (5%) was reserved as an unbiased test set for cross validation (R_{free}) for the model that eventually had an R_{work} of 16.1% and an R_{free} of 19.9%. The structure of the FtmOx1–α -KG binary complex and FtmOx1–fumitremorgin B complex were both solved by molecular replacement with the FtmOx1 structure as the initial model using Phaser in the CCP4 package[40,56–59]. The co-substrate α -KG and substrate fumitremorgin B were built using COOT followed by several rounds of refinement by PHENIX.Refine[49–55]. For the FtmOx1–α -KG complex, the final R_{work} was 20.3% with an R_{free} of 26.0%. For the FtmOx1–fumitremorgin B complex, the final R_{work} was refined to 16.7% and R_{free} to 20.3%. Model quality for all of the structures was evaluated with Ramachandran and MolProbity[51]. The structures show no outlier and most residues were in the favoured region of Ramachandran statistics (98.6% for apo FtmOx1, 98.1% for the FtmOx1–α -KG complex and 98.3% for FtmOx1–fumitremorgin B). When evaluated by MolProbity, all three structures rank 100% within the specific resolution range (apo FtmOx1 with a MolProbity score of 1.04, FtmOx1–α -KG complex 1.26 and FtmOx1–fumitremorgin B 1.12, respectively). Refinement statistics are summarized in Extended Data Table 1. Figure 2 and Extended Data Fig. 5 were prepared with PyMol[60].

Oxygen concentration determination for oxygenated buffer

Oxygen-saturated buffer[61] (10 ml) was transferred into syringes (12 cm^3) with a long needle, and the syringe was then sealed. An alkaline KI solution (2.1 M KI and 8.7 M KOH prepared using oxygen-free water) and $MnSO_4$ solution (2.1 M) in oxygen-free water were prepared in a Coy chamber and transferred out using syringes sealed by a rubber septum. The alkaline KI solution (0.2 ml) and the $MnSO_4$ solution (0.2 ml) were quickly aspirated into the syringe containing the 10 ml oxygen saturated buffer. Then, the syringe was quickly sealed again. The sample in the syringe was intensely mixed (turning the syringe ~10 times upside-down until the entire syringe was filled with the floating $Mn(OH)_3$ precipitate); the $Mn(OH)_3$ precipitate formed completely in 45 min according to the following reaction:

$$4Mn^{2+} + O_2 + 8OH^- + 2H_2O \rightarrow 4Mn(OH)_3 \downarrow \quad (1)$$

After 45 min, H_2SO_4 solution (0.2 ml, 2.7 M) was aspirated into the syringe, and Mn^{3+} ions oxidized iodide to iodine under acidic conditions according to the following reactions:

$$2Mn(OH)_3\,(s) + 3H_2SO_4 \rightarrow 2Mn^{3+} + 3SO_4^{2-} + 3H_2O \quad (2)$$

$$2Mn^{3+} + 2I^- \rightarrow 2Mn^{2+} + I_2 \quad (3)$$

Iodine eventually formed I_3^- ions with the excess KI:

$$I_2 + I^- \rightarrow I_3^- \quad (4)$$

The resulting iodine solution was transferred to a sample bottle and immediately titrated with standardized 2.5 mM $Na_2S_2O_3$ solution:

$$I_3^- + 2S_2O_3^{2-} \rightarrow 3I^- + S_4O_6^{2-} \quad (5)$$

According to reactions (1)–(5), one equivalent of oxygen molecule corresponds to four equivalents of $Na_2S_2O_3$. Therefore, the oxygen concentration in the oxygen-saturated buffer was determined based on the amount of standardized 2.5 mM $Na_2S_2O_3$ solution used for titration.

The $Na_2S_2O_3$ concentration was standardized with an iodine solution, which was prepared by mixing a standard KIO_3 solution and KI solution under acidic conditions

$$\left(KIO_3 + 5KI + 6H^+ \rightarrow 3I_2 + 6K^+ + 3H_2O;\quad I_2 + I^- \rightarrow I_3^-;\quad I_3^- + 2S_2O_3^{2-} \rightarrow 3I^- + S_4O_6^{2-}\right)$$

α-KG and oxygen stoichiometries in the FtmOx1 catalysis

To examine whether FtmOx1 is capable of catalysing verruculogen oxidation in the absence of other reductants, the FtmOx1 reaction was conducted under the following conditions: a 200 μ l anaerobic mixture in 100 mM Tris-HCl (pH 7.5), contained fumitremorgin B (360 μ M), α -KG (4 mM), and variable amounts of iron-loaded FtmOx1 (0.25× , 0.5× , 1× , and 2.0× of iron-loaded FtmOx1 relative to the fumitremorgin B concentration). The reaction was initiated by quickly mixing the above solution with 200 μ l oxygen-saturated buffer (1.2 mM) in the Coy chamber to make a solution containing 600 μ M oxygen. The final reaction mixture contained 180 μ M fumitremorgin B, 2 mM α -ketoglutarate, 600 μ M oxygen, and a variable amount of iron-loaded FmOx1 (0.25× , 0.5× , 1× , and 2× of FtmOx1 relative to that of verruculogen concentration). After the reaction was initiated, the reaction mixture was sealed and incubated for 0.5 h at 37 °C. The enzymatic reaction was quenched by adding 300 μ l chloroform, the precipitated protein was removed by centrifugation at 13,000 *g* for 10 min, and the chloroform layer was carefully removed. The reaction mixture was extracted one more time using a second 300-μ l volume of chloroform. The combined chloroform layers were concentrated by rotatory evaporation, and the residue was re-dissolved in 100 μ l acetonitrile and subjected to HPLC analysis.

To determine α -KG stoichiometry, 200 μ l anaerobic reaction mixture (in 100 mM Tris-HCl (pH 7.50)) contained 360 μ M fumitremorgin B, 240 μ M iron-loaded FtmOx1, and variable

amounts of α -KG. The concentration of α -KG was varied to make reaction mixtures containing 0.5× , 1.0× , 1.5× , and 2.0× of α -KG relative to the FtmOx1 concentration. The reaction was initiated by quickly mixing 200 μ l of oxygen-saturated buffer (1.2 mM) in the Coy chamber to make a final oxygen concentration of 600 μ M. The resulting reaction mixtures contained a final concentration of 180 μ M fumitremorgin B, 120 μ M iron-loaded FtmOx1, 600 μ M oxygen, and variable amounts of α -KG. After initiation, the reaction was sealed and incubated for 0.5 h at 37 °C. The enzymatic reaction was quenched by adding 300 μ l chloroform, the precipitated protein was removed by centrifugation at 13,000*g* for 10 min, and the chloroform layer was carefully removed. The reaction mixture was extracted one more time using a second 300-μ l volume of chloroform. The combined chloroform layers were concentrated by rotatory evaporation, and the residue was re-dissolved in 100 μ l of acetonitrile and subjected to HPLC analysis.

To determine oxygen stoichiometry, oxygen-saturated buffer was added to a 600 μ l anaerobic reaction mixture (100 mM Tris-HCl (pH 7.5) buffer, 360 μ M of fumitremorgin B, 240 μ M of iron-loaded FtmOx1, and 480 μ M of α -KG). To determine the amount of product formation under 1× of oxygen relative to iron-loaded FtmOx1 concentration, the above reaction mixture was quickly mixed with 120 μ l of oxygen-saturated buffer (1.2 mM) in the Coy chamber. To assess the amount of product formation under 2× of oxygen relative to iron-loaded FtmOx1 concentration, the above mixture was quickly mixed with 240 μ l of oxygen-saturated buffer (1.2 mM) in the Coy chamber. To determine the amount of production formation under 3× of oxygen relative to iron-loaded FtmOx1 concentration, the above mixture was quickly mixed with 360 μ l of oxygen-saturated buffer (1.2 mM) in the Coy chamber. After reaction initiation, the reaction mixtures were sealed and incubated for 0.5 h at 37 °C. The enzymatic reaction was quenched by adding 300 μ l chloroform, the precipitated protein was removed by centrifugation at 13,000 *g* for 10 min, and the chloroform layer was carefully separated. The reaction mixture was extracted one more time using a second 300-μ l volume of chloroform. The combined chloroform layers were concentrated by rotatory evaporation, and the residue was re-dissolved in 100 μ l of acetonitrile and subjected to HPLC analysis.

Reactions using Y224F-substituted FtmOx1

For the reactions using Y224F-substituted FtmOx1, the anaerobic reaction mixture (600 μ l, in 100 mM Tris-HCl (pH 7.5)) contained 400 μ M Y224F-substituted FtmOx1 containing 300 μ M Fe^{II}, 400 μ M fumitremorgin B, and 1,200 μ M α -KG. The reaction was initiated by quickly adding 400 μ l of oxygen-saturated buffer (1.2 mM) in the Coy chamber. The resulting reaction mixtures contained a final concentration of 240 μ M fumitremorgin B, 240 μ M Y224F-substituted FtmOx1 containing 192 μ M Fe^{II}, and 720 μ M α -KG. After initiation, the reaction mixture was sealed and incubated for 0.5 h at 37 °C. The enzymatic reaction was quenched by adding 300 μ l chloroform, the precipitated protein was removed by centrifugation at 13,000*g* for 10 min, and the chloroform layer was carefully separated. The reaction mixture was extracted once more using a second 300-μ l volume of chloroform. The combined chloroform layers were concentrated by rotatory evaporation, and the residue was re-dissolved in 100 μ l of acetonitrile and subjected to HPLC analysis.

Reactions using Y224A-substituted FtmOx1

Y224A-substituted FtmOx1 was analysed by a procedure similar to that described in 'Reactions using Y224F-substituted FtmOx1', except that Y224A-substituted FtmOx1 was used instead of Y224F-substituted FtmOx1.

HPLC analysis of the FtmOx1 reaction products

Enzymatic reaction products were routinely analysed by HPLC using a Phenomenex reversed phase C18 column (250 mm × 4 mm, 5 μ m; Phenomenex). A linear gradient of 30–100% (v/v) acetonitrile in water was run for 30 min with a flow rate of 0.7 ml min^{-1}, followed by 100% (v/v) acetonitrile for 5 min. Before the next injection, the column was equilibrated with 30% (v/v) acetonitrile for 2 min. The separation profile was monitored using a Photo Diode Array detector at 300 nm.

Products of the reaction (compounds **2** and **3**) using wild-type FtmOx1 were characterized by NMR and high-resolution mass spectrometry (see Supplementary Information).

Isolating products from reactions using wild-type, Y224F-, or Y224A-substituted FtmOx1

To characterize the reaction products, a large-scale reaction (270 ml) was performed using purified FtmOx1 (41.1 μ M) containing 32 μ M Fe^{II}, fumitremorgin B (30.9 μ M), and 60 μ M α -KG in Tris-HCl buffer (50 mm, pH 7.0) at 30 °C for 2 h. Chloroform (300 ml) was added to the reaction mixture. The chloroform layer was transferred into centrifuge bottles and centrifuged at 5,000 rpm for 10 min to remove precipitated proteins. The reaction mixture was extracted once more using a second 300-ml volume of chloroform. The combined chloroform layers were dried over Na_2SO_4 for 0.5 h and concentrated by rotatory evaporation. The residue was subjected to HPLC separation on a C18 column (4.6 × 150 mm). A linear gradient of 30–100% (v/v) acetonitrile in water was run for 25 min with a flow rate of 0.7 ml min^{-1}, followed by 100% (v/v) acetonitrile for 5 min. Before the next injection, the column was equilibrated with 30% (v/v) acetonitrile for 2 min. The elution was monitored using Photo Diode Array detector at 300 nm.

Products of the reaction using Y224F- and Y224A-substituted FtmOx1 variants (compounds **2**–**6**) were characterized using NMR and high-resolution mass spectrometry (see Supplementary Information).

Determining the α-KG dissociation constant

To maintain an anaerobic environment, all of the solutions were made anaerobically by several rounds of freeze-pump-thaw degassing. All spectroscopic studies used a 1-cm light path cuvette. After blanking against FtmOx1, spectra were recorded for samples to which anaerobic α -KG had been added. Titration plots were obtained by plotting the absorption at 520 nm. The titration data were fitted to equation (6)[62]

$$A_{obs}=A_{max}\left[\mathrm{E}-\mathrm{L}\right]/n\left[FtmOx1_{\mathrm{T}}\right] \quad (6)$$

in which the observed absorption (A_{obs}) was equal to the maximal absorption (A_{max}) multiplied by the concentration of enzyme–ligand complex ([E–L]) divided by the

concentration of ligand binding sites (the number (n) of ligands bound per subunit multiplied by the total concentration of FtmOx1 containing Fe^{II} ([$FtmOx1_T$])). The concentration of enzyme–ligand complex was obtained using equation (7)

$$[E-L]=\frac{(K_d+[\alpha-KG_T]+n[FtmOx1_T]\pm\sqrt{(K_d+[\alpha-KG_T]+n[FtmOx1_T])^2-4[\alpha-KG_T]n[FtmOx1_T]}}{2} \quad (7)$$

where K_d is the apparent ligand affinity and [α -KG_T] is the total α -KG concentration. The K_d values were determined from equations (6) and (7) using nonlinear curve fitting (OriginPro 8 software).

Self-hydroxylation in wild-type FtmOx1 protein

The FtmOx1 wild-type protein (0.6 mM) was mixed with (2.0 mM) α -KG in the anaerobic Coy chamber to form the pink species, and the UV–vis spectrum was recorded anaerobically using an S.I. Photonics CCD-440 spectrophotometer. All spectroscopic studies used a 1-cm light path cuvette. Upon exposing the above solution to O_2, the solution slowly changed to a blue colour, and the process was monitored using a Cary Bio UV–vis spectrometer.

Self-hydroxylation in FtmOx1(Y224F) variant

The Y224F-substituted FtmOx1 (1.1 mM) was mixed with α -KG (4.0 mM) in the anaerobic Coy chamber to form the binary complex (a pink species), and the UV spectrum was monitored anaerobically using an S.I. Photonics CCD-440 spectrophotometer. All spectroscopic studies used a 1-cm light path cuvette. Upon exposing the above solution to O_2, the solution slowly changed to a blue colour, and the process was monitored using a Cary Bio UV–vis spectrometer.

MS/MS analysis of FtmOx1

The following protein samples were analysed by tandem MS: (1) wild-type FtmOx1; (2) wild-type FtmOx1 treated with α -KG and oxygen; (3) Y224F-substituted FtmOx1; (4) Y224F-substituted FtmOx1 treated with α -KG and oxygen; and (5) Y224F-substituted FtmOx1 after single-turnover experiments in the presence of fumitremorgin B, α -KG, and oxygen. These protein samples (~ 1.5 nmol) were dissolved in 50 mM ammonium bicarbonate (pH 8.0) buffer to make a 50 μ l solution. Trypsin Gold (Promega US) was added to these solutions in a 1:50 (w/w) ratio, and the proteins were digested for 18 h at 37 °C. A C18 Ziptip (Millipore) was then used to desalt each peptide sample. Each digested sample (500 fmol) was injected and analysed by liquid chromatography (LC)–MS/MS on either an LTQ-Orbitrap XL mass spectrometer or a Q Exactive Plus Hybrid Quadrupole-Orbitrap mass spectrometer (Thermo Fisher Scientific) coupled with a Triversa Nanomate system (Advion Biosystems, Inc.), and a nanoACQUITY UPLC (Waters) with C18 reversed phase trap (2G-V/MTrap 5 μ m Symmetry C18 180 μ m × 20 mm) and analytical (1.7 μ m BEH130 C18 150 μ m × 100 mm) columns. Mobile phase A consisted of 98:2 water:ACN with 0.1% formic acid (FA) and mobile phase B contained 98:2 ACN:water with 0.1% FA. Peptide samples were loaded into the trap column at 2% B with a flow rate of 4.0 μ l min^{-1} for 4 min and then transferred to the analytical column at 0.5 μ l min^{-1}. The gradient was increased to 40% B over 40 min. For tandem MS analyses, data-dependent high resolution

higher-energy collisional dissociation mass spectra were acquired in the Orbitrap mass analysers and Xcalibur was used for data analysis. To identify target peptides, the ProteinProspector program from University of California, San Francisco was used to predict the potential product ions and match them to MS/MS product ions. The mass spectra were manually examined to verify the assignments.

Pre-steady-state characterization of FtmOx1

Stopped-flow experiments were performed on an Applied Photophysics SX20 stopped-flow spectrometer operating in an MBraun UNilab glove box. To maintain an anaerobic environment, all of the solutions were prepared in an inert atmosphere box. An oxygen-saturated buffer solution (100 mM Tris-HCl (pH 7.5)) was mixed with an equal volume of an oxygen-free solution containing FtmOx1 (0.65 mM), Fe^{II} (0.58 mM), α -KG (12 mM), substrate (0.58 mM), and 20% glycerol to initiate the reaction. Absorbance scans from 300 to 700 nm were collected with a diode-array detector at 8 °C. The resulting data were processed using SigmaPlot software.

Freeze-quench experiments were performed using a KinTek quench-flow instrument. Analogous to the stopped-flow experiments, an oxygen-saturated buffer solution (100 mM Tris-HCl (pH 7.5)) was mixed with an equal volume of an oxygen-free solution containing FtmOx1 (0.65 mM), Fe^{II} (0.58 mM), α -KG (12 mM), substrate (0.58 mM), and 20% glycerol to initiate the reaction at 8 °C. The resulting reaction was terminated by injection of the solution into liquid ethane (−90 °C) at various time points. The reaction time of a freeze-quenched sample is the sum of the ageing time and the quench time. The ageing time was the transit time for the reaction mixture through the ageing hose. The quench time corresponded to the time required after injection into the cryosolvent for the reaction mixture to be cooled sufficiently to prevent further reaction and was estimated as ~5 ms (ref. 63).

The chemical-quench-flow experiments were performed using a KinTek quench-flow instrument. Analogous to the freeze-quench experiments, an oxygen-saturated buffer solution (100 mM Tris-HCl (pH 7.5)) was mixed with an equal volume of an oxygen-free solution containing FtmOx1 (0.65 mM), Fe^{II} (0.58 mM), α -KG (12 mM), substrate (0.58 mM), and 20% glycerol to initiate the reaction at 8 °C. The resulting reaction was terminated by injecting the solution into a microcentrifuge tube containing 4× volumes of acetone at the desired reaction times. Before HPLC analysis, the samples were centrifuged to remove protein, and the supernatant was concentrated by rotatory evaporation. The concentrated samples were subjected to HPLC separation on a C18 column (4.6 × 100 mm). A linear gradient of 30–100% (v/v) acetonitrile in water was run for 25 min with a flow rate of 0.5 ml min^{-1}, followed by 100% (v/v) acetonitrile for 3 min. Before the next injection, the column was equilibrated with 30% (v/v) acetonitrile for 2 min. The substances were detected with a Photo Diode Array detector at 300 nm.

X-band (9.64 GHz) EPR spectra were recorded on a Bruker E500A spectrometer equipped with an Oxford ESR 910 cryostat for low-temperature measurements. The microwave frequency was calibrated with a frequency counter, and the magnetic field was calibrated with an NMR gaussmeter. The temperature of the X-band cryostat was calibrated with a

carbon-glass resistor temperature probe (CGR-1-1000 LakeShore Cryotronics). For all EPR spectra, a modulation frequency and amplitude of 100 kHz and 1 mT were used. The EPR spectral simulations were performed using the simulation software Spin Count developed by one of the authors.

Extended Data

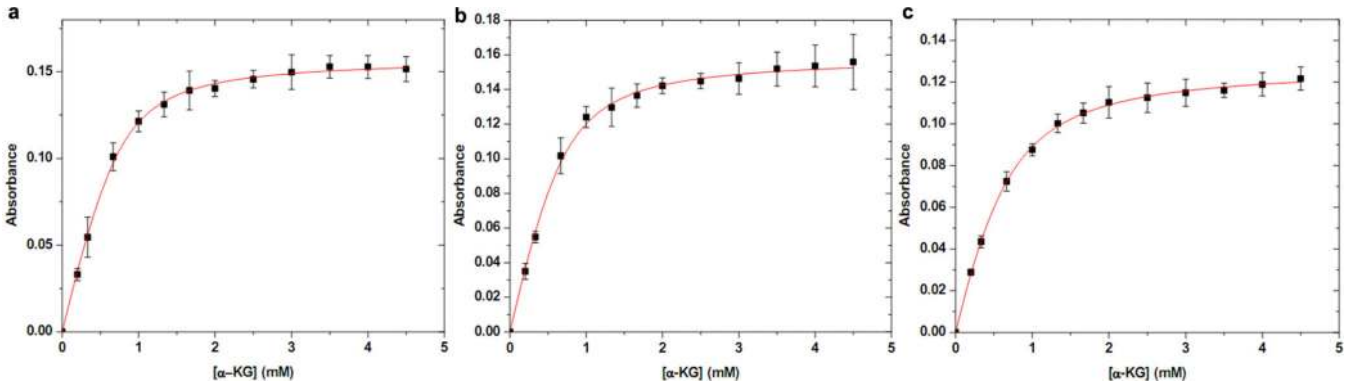

Extended Data Figure 1. Characterization of FtmOx1–α-KG complex

a, Wild-type FtmOx1 and α -KG binding curve. The increase in absorbance at 520 nm as a function of α -KG concentration when it was added to a solution of wild-type FtmOx1 (0.9 mM) and Fe^{II} (0.72 mM) is plotted. On the basis of the equations described in the Methods (determining the α -KG dissociation constant), the K_d for wild-type FtmOx1 and α -KG is ~ 185 ± 35 μ M. **b**, Y224F-substituted FtmOx1 and α -KG binding curve. The increase of absorbance at 520 nm as a function of α -KG concentration when it was added to a solution of Y224F-substituted FtmOx1 (0.9 mM) and Fe^{II} (0.7 mM) is plotted. K_d for Y224F-substituted FtmOx1 and α -KG is ~ 198 ± 58 μ M. **c**, Y224A-substituted FtmOx1 and α -KG binding curve. The increase of absorbance at 520 nm as a function of α -KG concentration when it was added to a solution of Y224A-substituted FtmOx1 (0.7 mM) and Fe^{II} (0.51 mM) is plotted. K_d for Y224A-substituted FtmOx1 and α -KG is 204 ± 43 μ M. In **a**–**c**, the K_d was calculated based on the concentration of iron-loaded FtmOx1. The experiments were replicated three times and error bars represent s.e.m.

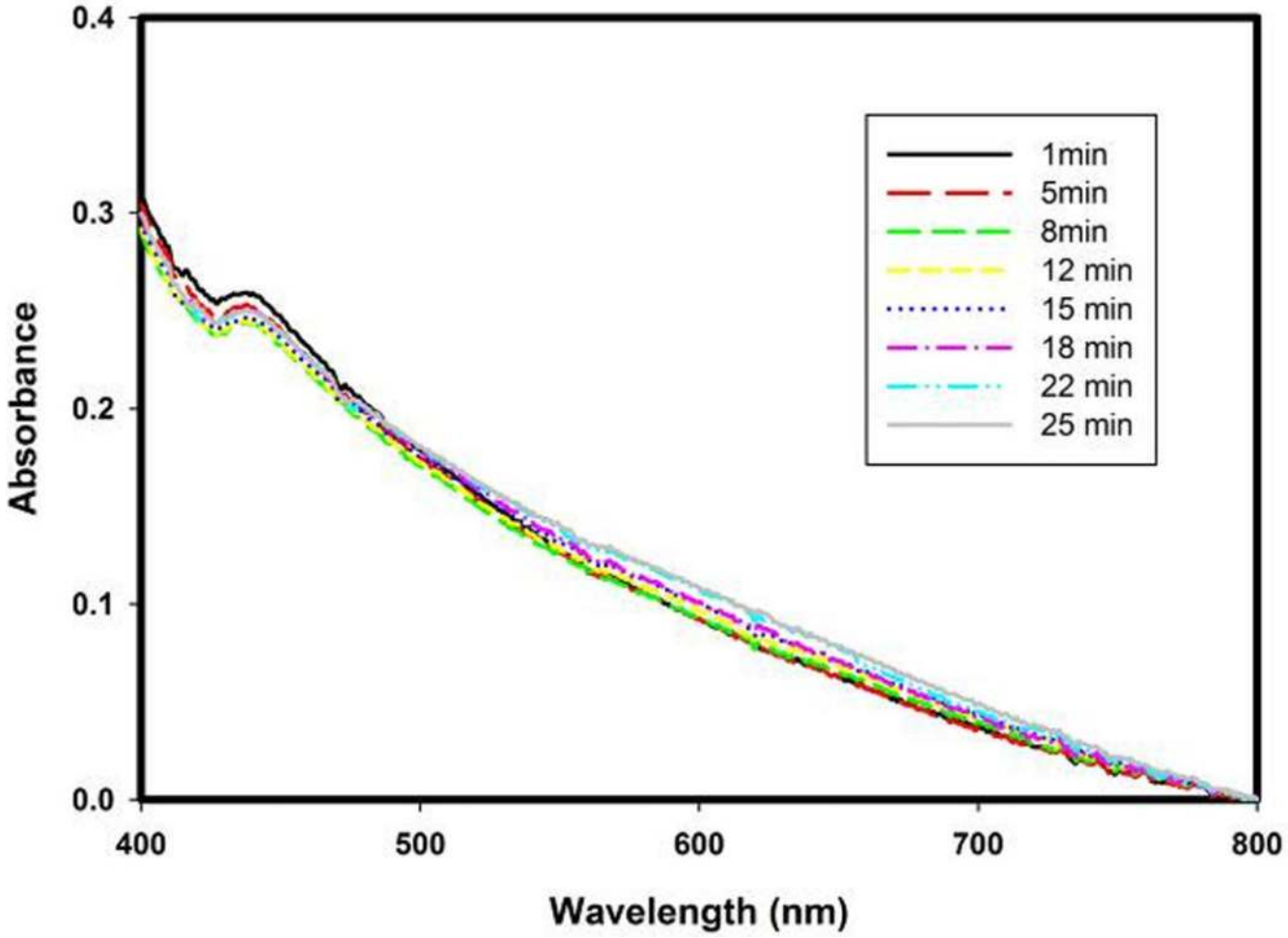

Extended Data Figure 2. Suppression of DOPA formation by the presence of substrate fumitremorgin B

There is no immediate evidence for the formation of DOPA upon the exposure of the FtmOx1–α -KG complex to O_2 when the substrate fumitremorgin B is present. Spectra were recorded after FtmOx1 was used as the control to blank the UV–visible absorption reading.

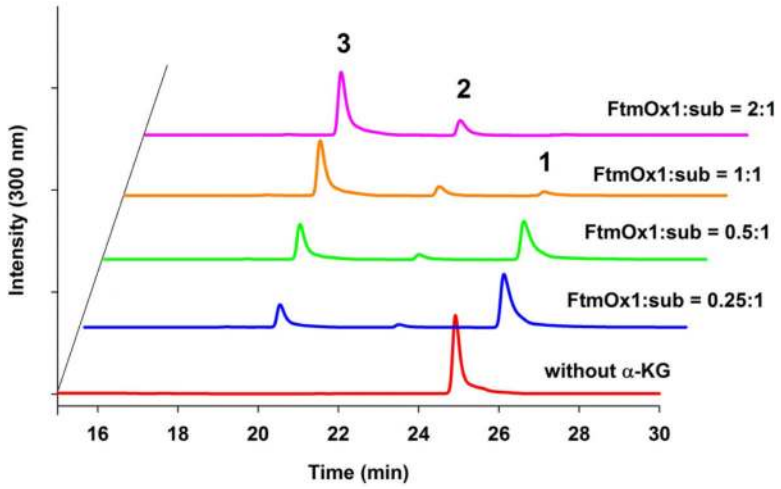

Extended Data Figure 3. HPLC chromatograms of the FtmOx1 reaction enzyme-concentration dependence

Chromatograms of FtmOx1 reactions with increasing amounts of FtmOx1 relative to the amount of substrate. The reaction mixture contained 100 mM Tris-HCl, (pH 7.5), 180 μ M fumitremorgin B, 2 mM α -ketoglutarate, and variable amounts of FmOx1. Identities of the peaks were assigned based on subsequent NMR and MS characterizations of the isolated compounds. This experiment indicates that FtmOx1 is capable of catalysing endoperoxides formation in the absence of any other reductants.

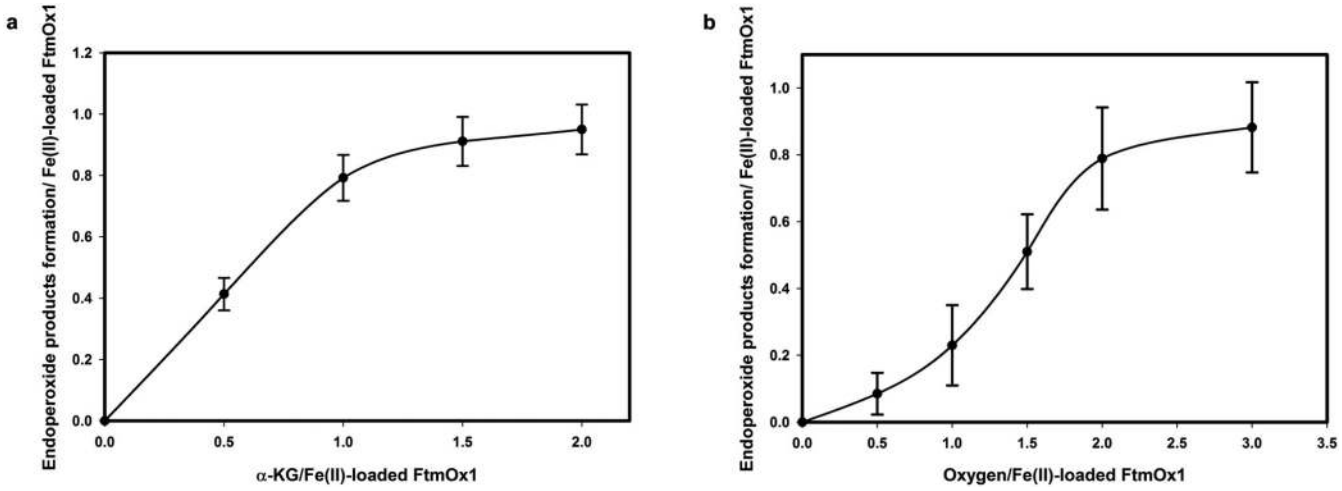

Extended Data Figure 4. Stoichiometry determination for α-KG and O_2 in FtmOx1 reaction

a, **b**, Equivalents of endoperoxide products (**2** and **3**) produced as a function of the ratio of α -KG to iron-loaded FtmOx1 (**a**) and oxygen to iron-loaded FtmOx1 (**b**). The quantification was conducted based on the fumitremorgin B (**1**), compound **2**, and compound **3** internal standards. All calculations were based on the concentration of iron-loaded FtmOx1. The experiments were replicated three times and error bars represent s.d.

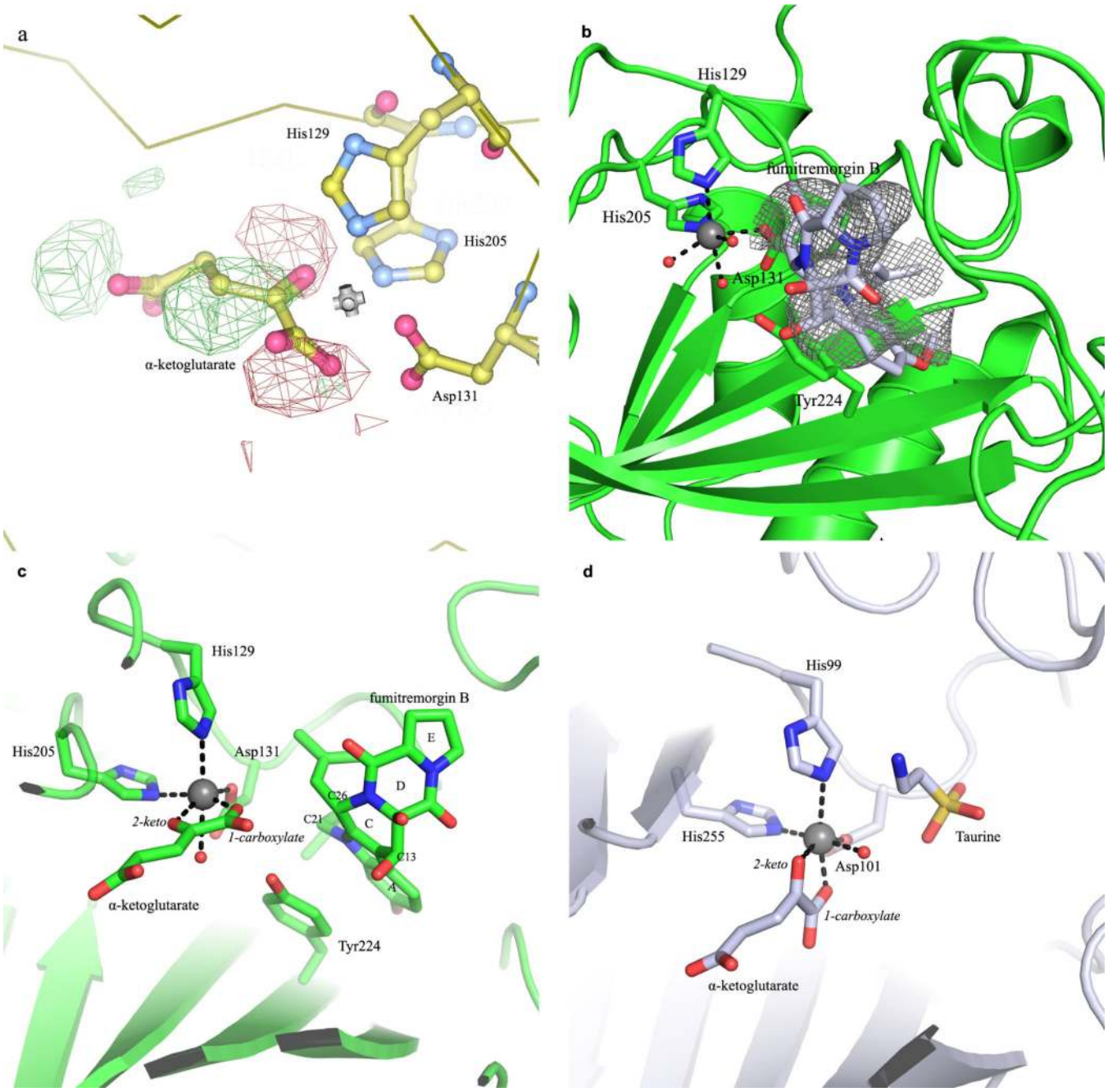

Extended Data Figure 5. Structural comparison of the active site topologies between FtmOx1 and TauD

a, Examination of the alternative configuration of α -KG in the FtmOx1–α -KG binary complex using the configuration of α -KG in the TauD–α -KG binary complex. We modelled α -KG in this alternative binding mode and calculated the difference map. In the $F_o - F_c$ map, strong positive density (green) and negative density (red) are shown even when contoured to high level (3.3σ), indicating that this configuration is not correct for the FtmOx1–α -KG complex. **b**, The $F_o - F_c$ map at the active site of the FtmOx1–fumitremorgin B complex. A model of the substrate fumitremorgin B is superimposed onto

the difference map, which is contoured at 2.8σ. **c**, Side-by-side comparison of FtmOx1 and TauD active-site topologies. In the left panel, the superimposition of the binary structures of FtmOx1–α -KG and FtmOx1–fumitremorgin-B (**1**) show that the remaining site for oxygen binding and activation is blocked from the substrate by Y224. **d**, In contrast, in the structure of the TauD–taurine–α -KG tertiary complex, the remaining site for O_2 binding and activation directly faces the substrate (taurine).

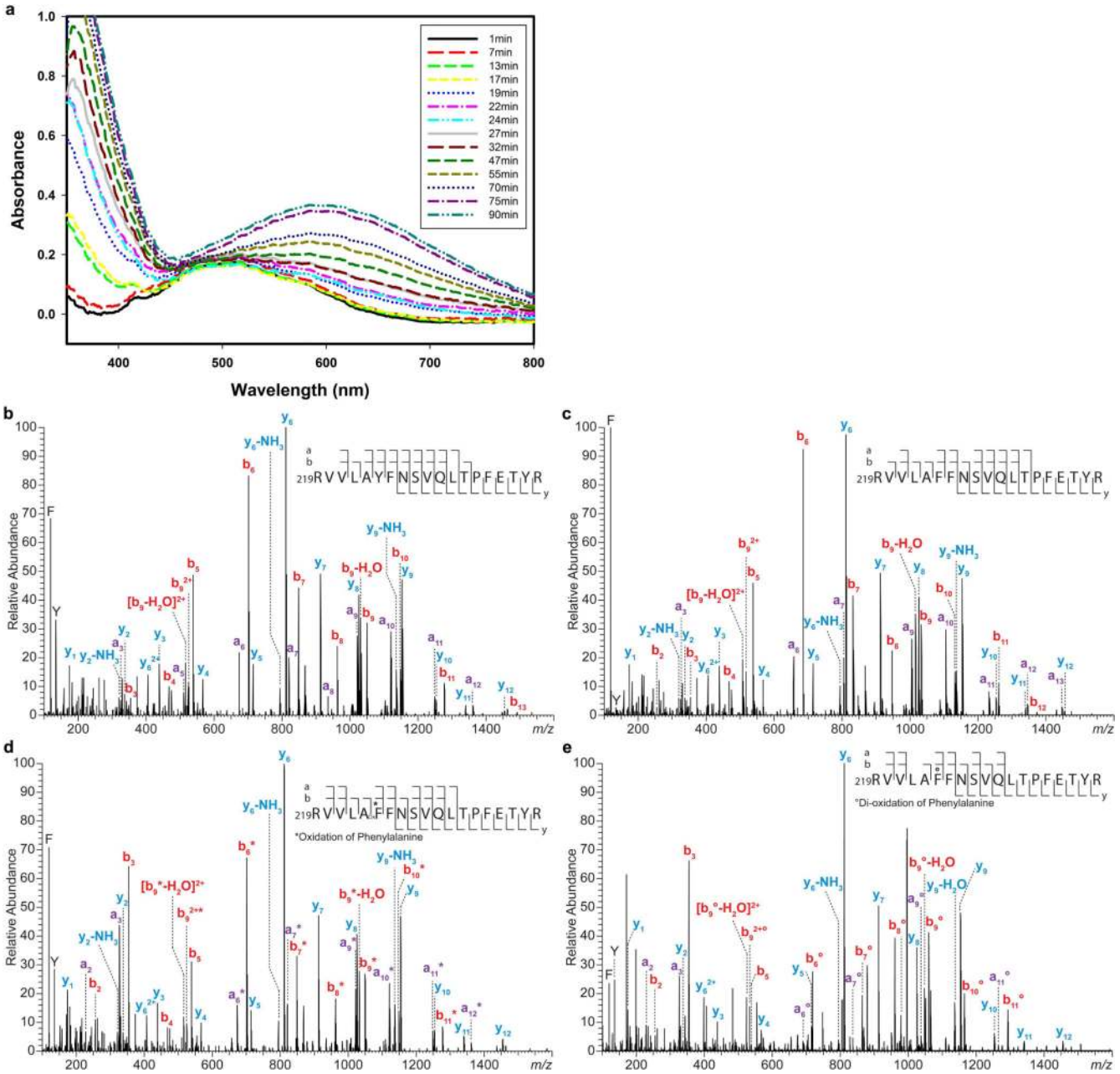

Extended Data Figure 6. Characterization of FtmOx1 Y224F variant

a, Self-hydroxylation reaction in Y224F-substituted FtmOx1. Formation of DOPA upon exposure of the Y224F-substituted FtmOx1–α -KG complex to O_2. **b**–**e**, MS/MS analyses of

Y224F-substituted FtmOx1. **b**, MS/MS spectrum of the triply charged parent ion at *m/z* 768.4109 of a tryptic digested peptide (residue 219–237) from wild-type FtmOx1. **c**, MS/MS spectrum of the triply charged parent ion at *m/z* 763.0793 of a tryptic digested peptide (residue 219–237) from Y224F-substituted FtmOx1. **d**, MS/MS spectrum of the triply charged parent ion at *m/z* 768.4109 of a tryptic digested peptide (residue 219–237) after exposure Y224F(FtmOx1)–α -KG tertiary complex to O_2. **e**, MS/MS spectrum of the triply charged parent ion at *m/z* 773.7426 of a tryptic digested peptide (residue 219–237) for DOPA formed upon exposure of FtmOx(Y224F)–α -KG complex to O_2 in the absence substrate fumitremorgin B.

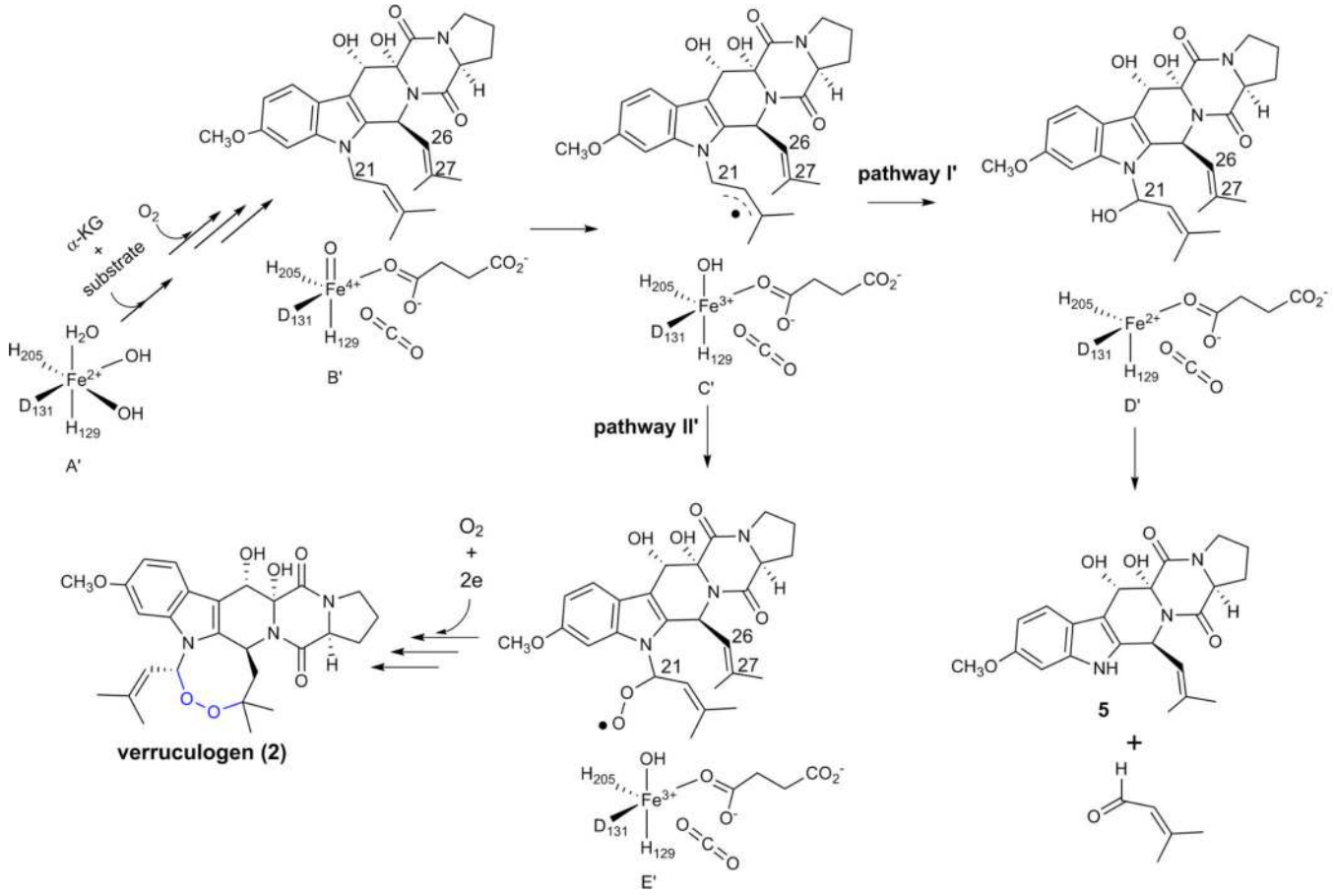

Extended Data Figure 7.
Mechanistic model for the production of dealkylation products in FtmOx1 Y224A or Y224F variants.

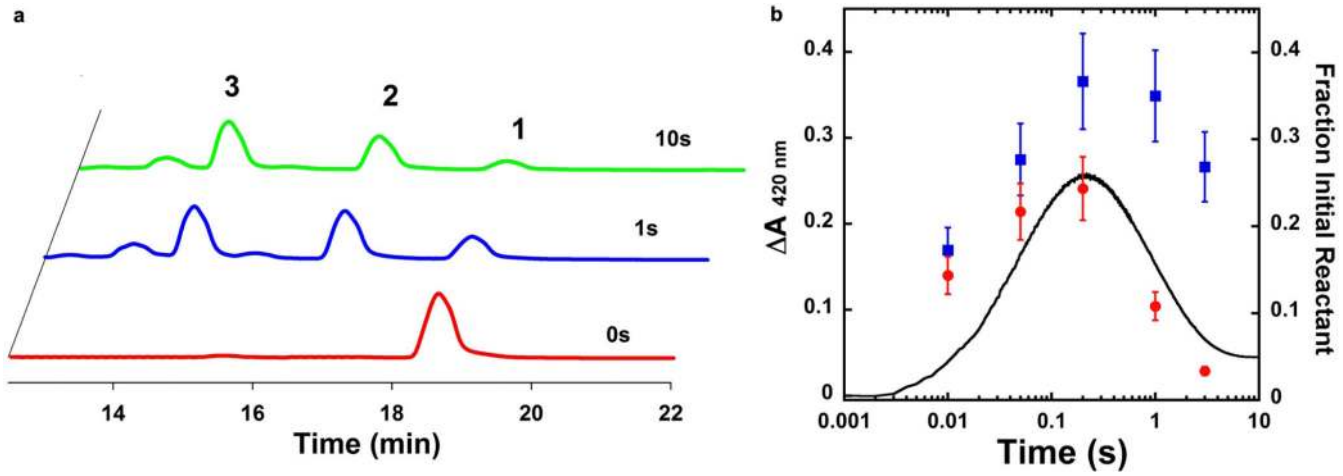

Extended Data Figure 8. Pre-steady-state analyses of FtmOx1 reactions

a, HPLC chromatograms for FtmOx1 reactions chemically quenched at the indicated times. The reaction mixture in 100 mM Tris-HCl (pH 7.5) buffer contained FtmOx1 (0.65 mM), Fe^{II} (0.58 mM), α -KG (12 mM), substrate (0.58 mM), and 20% glycerol. The mixture was mixed with O_2-saturated buffer to initiate the reaction. There is an extra signal next to compound **3**, which might be due to other chemicals released during the quench process. Results from the chemical quench experiment indicate that FtmOx1 catalysis is on the timescale of a few seconds per cycle. **b**, Time-dependent 420 nm absorption change (black solid curve) determined by stopped-flow optical absorption spectroscopy and the concentrations of the high-spin Fe^{3+} species (blue squares) and the $g = 2$ species (red dots) determined in the rapid-freeze-quench EPR experiments. The black solid curve is associated with the left *y* axis and is from the average of two stopped-flow trials. The blue squares and red dots are associated with the right *y* axis and are from the average of two rapid-freeze-quench EPR experiments. The experiments were repeated twice, and error bars reflect the uncertainty of the packing factor of rapid-freeze-quench EPR samples, which is around ± 10%.

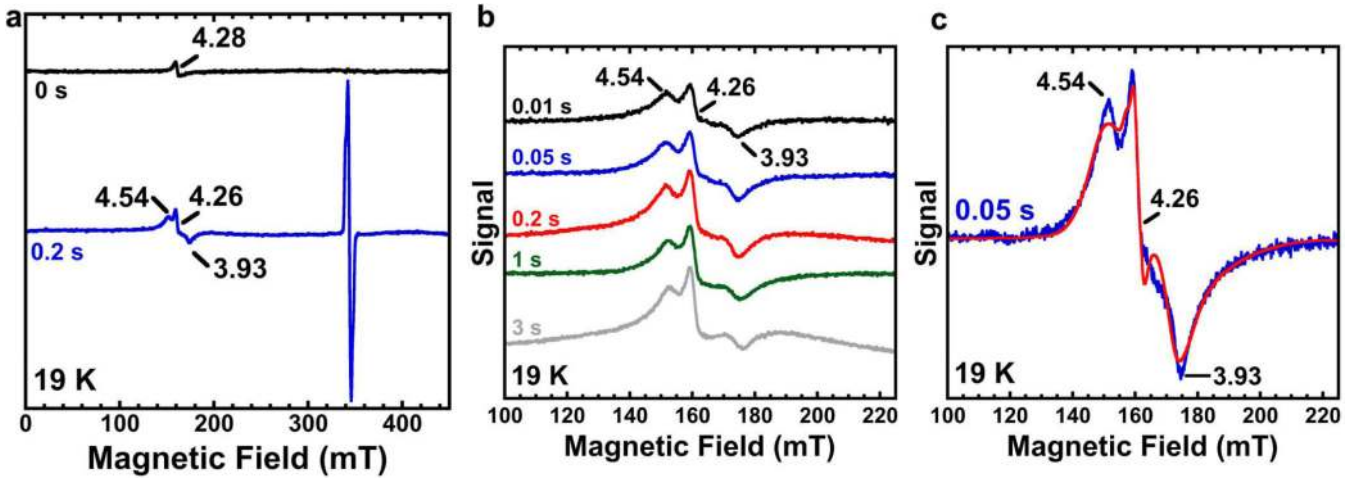

Extended Data Figure 9. EPR spectroscopic analyses of FtmOx1 reactions

a, X-band EPR spectra measured at 19 K in reaction samples prepared at the indicated times. The black line shows the sample containing the FtmOx1–Fe^{II}–α -KG complex in the absence of O_2. (There is a very small signal at $g \approx 4.3$ region, only accounted for by <5 μ M iron in the sample, which might be due to a very small amount of Fe^{3+} from inactive enzyme.) Bottom, the reaction sample freeze-quenched at ~0.2 s after mixing the FtmOx1–Fe^{II}–α -KG complex with O_2. It has two signals: an Fe^{3+} (g = 4.54, 4.26, and 3.93) and a radical signal at the g = 2 region. **b**, X-band EPR spectra measured at 19 K for samples freeze-quenched at the indicated times showing the formation of high-spin ferric species on the time scale within 1 s. The reaction was initiated by mixing the FtmOx1–Fe^{II}–α -KG complex with O_2. g-values are indicated in the figure. **c**, X-band EPR spectra measured at 19 K for samples freeze-quenched at 0.05 s and the spectral simulation for an S = 5/2 high-spin ferric species. The simulation parameters are: D = 0.3 cm^{-1}, E/D = 0.266, $\sigma(E/D)$ = 0.03, and g = 4.54, 4.26, 3.93. Measurement conditions in **a**–**c**: microwave frequency, 9.64 GHz; microwave power, 0.2 mW; modulation amplitude, 1 mT; and modulation frequency, 100 kHz.

Extended Data Table 1

X-ray crystallography data collection and refinement statistics

	FtmOxl		FtmOxl•α-KG Complex	FtmOxl•fumitremorgin B complex
Data collection	Set-Met	Native		
Space group	P 1 2_1 1	P 1 2_1 1	P 1 2_1 1	P 1 2_1 1
Cell dimensions				
a, *b*, *c* (Å)	60.6, 45.8, 105.2	60.4, 45.6, 105.4	60.6, 45.8, 105.4	60.3, 45.4, 104.8
α, *β*, *γ* (°)	90.0, 100.5, 90.0	90.0, 99.7, 90.0	90.0, 100.0, 90.0	90.0, 100.3, 90.0
Resolution (Å)	48.23 - 3.49 (3.63 - 3.51)*	42.91 - 1.95 (2.02 - 1.95)	36.13 - 2.54 (2.63 - 2.54)	36.05 - 2.11 (2.19 - 2.11)
R_{sym}	0.114 (0.157)	0.101 (0.725)	0.125 (0.691)	0.077 (0.338)
$I/\sigma I$	13.19 (7.64)	18.33 (2.02)	10.53 (1.50)	17.08 (2.80)
Completeness (%)	99.90 (100.00)	99.90 (99.22)	99.93 (99.35)	99.86 (98.63)
Redundancy	6.1 (3.2)	6.6 (5.7)	3.7 (3.7)	3.7 (3.1)
Refinement				
Resolution (Å)		42.91 - 1.95 (2.02 - 1.95)	36.13 - 2.54 (2.63 - 2.54)	36.05 - 2.11 (2.19 - 2.11)
No. reflections		41711	18951	32435
R_{work}/R_{free}		0.1643/0.2043	0.1756/0.2340	0.1670/0.2033
No. atoms		4906	4704	4884
Protein		4535	4535	4535
Ligand/ion		25	23	38
Water		346	146	311
B-factors ($Å^2$)		29.5	35.8	32.4
Protein		29.2	35.8	31.9
Ligand/ion		47.5	41.0	49.6
Water		32.0	35.3	37.2

	FtmOxI	FtmOxI•α-KG Complex	FtmOxI•fumitremorgin B complex
R.m.s deviations			
Bond lengths (Å)	0.005	0.017	0.004
Bond angles (°)	0.97	0.93	0.87

* Highest resolution shell is shown in parenthesis.

Supplementary Material

Refer to Web version on PubMed Central for supplementary material.

Acknowledgements

We thank H.-w. Liu, S. Elliott and A. Liu for comments on the manuscript. We also thank R. Fan and J. Lee for assistance with the pre-steady state kinetics studies, J. Caradonna for use of stopped-flow instruments, and A. Monzingo for assistance with crystallography software. This work is supported in part by grants from the National Institutes of Health (R01 GM093903 to P.L.; P41 GM104603 to C.E.C.; R01 GM104896 to Y.J.Z.; and R01 GM077387 to M.P.H.), the National Science Foundation (CHE-1309148 to P.L.; CHE-1126268 for the EPR spectrometer), the Welch Foundation (F-1778 to Y.J.Z.), the 973 program (2013CB734000 to L.Z), and Y.G. acknowledges financial support from Carnegie Mellon University. Crystallographic data collection was conducted at advanced light sources (Beamline 5.0.3) and advanced photon sources (BL23-ID-B), Department of Energy (DOE) National User Facility. L.Z. is an awardee of the National Distinguished Young Scholar Program in China (31125002).

References

1. Casteel DA. Peroxy natural products. Nat. Prod. Rep. 1992; 9:289–312. [PubMed: 1522977]
2. Casteel DA. Peroxy natural products. Nat. Prod. Rep. 1999; 16:55–73.
3. Chaturvedi D, Goswami A, Saikia PP, Barua NC, Rao PG. Artemisinin and its derivatives: a novel class of anti-malarial and anti-cancer agents. Chem. Soc. Rev. 2010; 39:435–454. [PubMed: 20111769]
4. Paddon CJ, Keasling JD. Semi-synthetic artemisinin: a model for the use of synthetic biology in pharmaceutical development. Nature Rev. Microbiol. 2014; 12:355–367. [PubMed: 24686413]
5. Dembitsky VM. Bioactive peroxides as potential therapeutic agents. Eur. J. Med. Chem. 2008; 43:223–251. [PubMed: 17618015]
6. Widboom PF, Fielding EN, Liu Y, Bruner SD. Structural basis for cofactor-independent dioxygenation in vancomycin biosynthesis. Nature. 2007; 447:342–345. [PubMed: 17507985]
7. Steiner RA, Janssen HJ, Roversi P, Oakley AJ, Fetzner S. Structural basis for cofactor-independent dioxygenation of N-heteroaromatic compounds at the α /β -hydrolase fold. Proc. Natl Acad. Sci. USA. 2010; 107:657–662. [PubMed: 20080731]
8. Thierbach S, et al. Substrate-assisted O_2 activation in a cofactor-independent dioxygenase. Chem. Biol. 2014; 21:217–225. [PubMed: 24388758]
9. Marnett LJ. Cyclooxygenase mechanisms. Curr. Opin. Chem. Biol. 2000; 4:545–552. [PubMed: 11006543]
10. Grundmann A, Li SM. Overproduction, purification and characterization of FtmPT1, a brevianamide F prenyltransferase from Aspergillus fumigatus. Microbiology. 2005; 151:2199–2207. [PubMed: 16000710]
11. Steffan N, Grundmann A, Afiyatullov S, Ruan H, Li SM. FtmOx1, a non-heme Fe(II) and α -ketoglutarate-dependent dioxygenase, catalyses the endoperoxide formation of verruculogen in Aspergillus fumigatus. Org. Biomol. Chem. 2009; 7:4082–4087. [PubMed: 19763315]
12. Kato N, et al. Gene disruption and biochemical characterization of verruculogen synthase of Aspergillus fumigatus. ChemBioChem. 2011; 12:711–714. [PubMed: 21404415]

13. Clifton IJ, et al. Structural studies on 2-oxoglutarate oxygenases and related double-stranded α -helix fold proteins. J. Inorg. Biochem. 2006; 100:644–669. [PubMed: 16513174]
14. Hausinger RP. Fe(II)/α -ketoglutarate-dependent hydroxylases and related enzymes. Crit. Rev. Biochem. Mol. Biol. 2004; 39:21–68. [PubMed: 15121720]
15. Costas M, Mehn MP, Jensen MP, Que L. Dioxygen activation at mononuclear nonheme iron active sites: Enzymes, models, and intermediates. Chem. Rev. 2004; 104:939–986. [PubMed: 14871146]
16. Solomon EI, et al. Geometric and electronic structure/function correlations in non-heme iron enzymes. Chem. Rev. 2000; 100:235–350. [PubMed: 11749238]
17. Kovaleva EG, Lipscomb JD. Versatility of biological non-heme Fe(II) centers in oxygen activation reactions. Nature Chem. Biol. 2008; 4:186–193. [PubMed: 18277980]
18. Ryle MJ, Padmakumar R, Hausinger RP. Stopped-flow kinetic analysis of *Escherichia coli* taurine/α -ketoglutarate dioxygenase: interactions with α -ketoglutarate, taurine, and oxygen. Biochemistry. 1999; 38:15278–15286. [PubMed: 10563813]
19. Liu A, Ho RYN, Que L. Alternative reactivity of an α -ketoglutarate-dependent Iron(II) oxygenase: enzyme self-hydroxylation. J. Am. Chem. Soc. 2001; 123:5126–5127. [PubMed: 11457355]
20. Volkamer A, Kuhn D, Grombacher T, Rippmann F, Rarey M. Combining global and local measures for structure-based druggability predictions. J. Chem. Inf. Model. 2012; 52:360–372. [PubMed: 22148551]
21. Elkins JM, et al. X-ray crystal structure of *Escherichia coli* taurine/α -ketoglutarate dioxygenase complexed to ferrous iron and substrates. Biochemistry. 2002; 41:5185–5192. [PubMed: 11955067]
22. Liu P, et al. Protein purification and function assignment of the epoxidase catalyzing the formation of fosfomycin. J. Am. Chem. Soc. 2001; 123:4619–4620. [PubMed: 11457256]
23. Vaillancourt FH, Yeh E, Vosburg DA, O'Connor SE, Walsh CT. Cryptic chlorination by a non-haem iron enzyme during cyclopropyl amino acid biosynthesis. Nature. 2005; 436:1191–1194. [PubMed: 16121186]
24. Blasiak LC, Vaillancourt FH, Walsh CT, Drennan CL. Crystal structure of the non-haem iron halogenase SyrB2 in syringomycin biosynthesis. Nature. 2006; 440:368–371. [PubMed: 16541079]
25. Clifton IJ, et al. Crystal structure of carbapenem synthase (CarC). J. Biol. Chem. 2003; 278:20843–20850. [PubMed: 12611886]
26. Chang WC, et al. Mechanism of the C5 stereoinversion reaction in the biosynthesis of carbapenem antibiotics. Science. 2014; 343:1140–1144. [PubMed: 24604200]
27. Blodgett JAV, et al. Unusual transformations in the biosynthesis of the antibiotic phosphinothricin tripeptide. Nature Chem. Biol. 2007; 3:480–485. [PubMed: 17632514]
28. Krebs C, Galonic Fujimori D, Walsh CT, Bollinger JM Jr. Non-heme Fe(IV)-oxo intermediates. Acc. Chem. Res. 2007; 40:484–492. [PubMed: 17542550]
29. Stubbe J, van der Donk WA. Protein radicals in enzyme catalysis. Chem. Rev. 1998; 98:705–762. [PubMed: 11848913]
30. Minor, W.; Otwinowski, Z. Methods in Enzymology, Macromolecular Crystallography. Academic Press; 1997.
31. Adams PD, et al. PHENIX: a comprehensive Python-based system for macromolecular structure solution. Acta Crystallogr. D. 2010; 66:213–221. [PubMed: 20124702]
32. Terwilliger TC. Maximum-likelihood density modification. Acta Crystallogr. D. 2000; 56:965–972. [PubMed: 10944333]
33. Terwilliger TC, et al. Decision-making in structure solution using Bayesian estimates of map quality: the PHENIX AutoSol wizard. Acta Crystallogr. D. 2009; 65:582–601. [PubMed: 19465773]
34. Baker D, Bystroff C, Fletterick RJ, Agard DA. PRISM: topologically constrained phased refinement for macromolecular crystallography. Acta Crystallogr. D. 1993; 49:429–439. [PubMed: 15299502]

35. Bricogne G. Geometric sources of redundancy in intensity data and their use for phase determination. Acta Crystallogr. A. 1974; 30:395–405.
36. Brünger AT. Free R value: a novel statistical quantity for assessing the accuracy of crystal structures. Nature. 1992; 355:472–475. [PubMed: 18481394]
37. Cowtan K. Error estimation and bias correction in phase-improvement calculations. Acta Crystallogr. D. 1999; 55:1555–1567. [PubMed: 10489450]
38. Cowtan KD, Main P. Improvement of macromolecular electron-density maps by the simultaneous application of real and reciprocal space constraints. Acta Crystallogr. D. 1993; 49:148–157. [PubMed: 15299555]
39. Cowtan KD, Main P. Phase combination and cross validation in iterated density-modification calculations. Acta Crystallogr. D. 1996; 52:43–48. [PubMed: 15299724]
40. Winn MD, et al. Overview of the CCP4 suite and current developments. Acta Crystallogr. D. 2011; 67:235–242. [PubMed: 21460441]
41. Sayre D. Least-squares phase refinement. II. High-resolution phasing of a small protein. Acta Crystallogr. A. 1974; 30:180–184.
42. Schuller DJ. MAGICSQUASH: more versatile non-crystallographic averaging with mulitple constraints. Acta Crystallogr. D. 1996; 52:425–434. [PubMed: 15299663]
43. Swanson SM. Core tracing: depicting connections between features in electron density. Acta Crystallogr. D. 1994; 50:695–708. [PubMed: 15299367]
44. Wang BC. Resolution of phase ambiguity in macromolecular crystallography. Methods Enzymol. 1985; 115:90–112. [PubMed: 4079800]
45. Zhang K, Main P. The use of Sayre's equation with solvent flattening and histogram matching for phase extension and refinement of protein structures. Acta Crystallogr. A. 1990; 46:377–381.
46. Cowtan K. The Buccaneer software for automated model building. 1. Tracing protein chains. Acta Crystallogr. D. 2006; 62:1002–1011. [PubMed: 16929101]
47. Cowtan K. Fitting molecular fragments into electron density. Acta Crystallogr. D. 2008; 64:83–89. [PubMed: 18094471]
48. Emsley P, Lohkamp B, Scott WG, Cowtan K. Features and development of Coot. Acta Crystallogr. D. 2010; 66:486–501. [PubMed: 20383002]
49. Afonine PV, et al. Towards automated crystallographic structure refinement with phenix.refine. Acta Crystallogr. D. 2012; 68:352–367. [PubMed: 22505256]
50. Berkholz DS, Shapovalov MV, Dunbrack RL Jr, Karplus PA. Conformation dependence of backbone geometry in proteins. Structure. 2009; 17:1316–1325. [PubMed: 19836332]
51. Chen VB, et al. MolProbity: all-atom structure validation for macromolecular crystallography. Acta Crystallogr. D. 2010; 66:12–21. [PubMed: 20057044]
52. Headd JJ, et al. Use of knowledge-based restraints in phenix.refine to improve macromolecular refinement at low resolution. Acta Crystallogr. D. 2012; 68:381–390. [PubMed: 22505258]
53. Moriarty NW, Grosse-Kunstleve RW, Adams PD. electronic Ligand Builder and Optimization Workbench (eLBOW): a tool for ligand coordinate and restraint generation. Acta Crystallogr. D. 2009; 65:1074–1080. [PubMed: 19770504]
54. Tronrud DE, Berkholz DS, Karplus PA. Using a conformation-dependent stereochemical library improves crystallographic refinement of proteins. Acta Crystallogr. D. 2010; 66:834–842. [PubMed: 20606264]
55. Urzhumtseva L, Afonine PV, Adams PD, Urzhumtsev A. Crystallographic model quality at a glance. Acta Crystallogr. D. 2009; 65:297–300. [PubMed: 19237753]
56. McCoy AJ, et al. Phaser crystallographic software. J. Appl. Crystallogr. 2007; 40:658–674. [PubMed: 19461840]
57. McCoy AJ, Grosse-Kunstleve RW, Storoni LC, Read RJ. Likelihood-enhanced fast translation functions. Acta Crystallogr. D. 2005; 61:458–464. [PubMed: 15805601]
58. Read RJ. Pushing the boundaries of molecular replacement with maximum likelihood. Acta Crystallogr. D. 2001; 57:1373–1382. [PubMed: 11567148]
59. Storoni LC, McCoy AJ, Read RJ. Likelihood-enhanced fast rotation functions. Acta Crystallogr. D. 2004; 60:432–438. [PubMed: 14993666]

60. Schrodinger LLC. The PyMOL Molecular Graphics System, Version 1.3r1. 2010

61. Helm I, Jalukse L, Vilbaste M, Leito I. Micro-Winkler titration method for dissolved oxygen concentration measurement. Anal. Chim. Acta. 2009; 648:167–173. [PubMed: 19646580]

62. Ryle MJ, Padmakumar R, Hausinger RP. Stopped-flow kinetic analysis of *Escherichia coli* taurine/α -ketoglutarate dioxygenase: interactions with α -ketoglutarate, taurine, and oxygen. Biochemistry. 1999; 38:15278–15286. [PubMed: 10563813]

63. Baldwin J, et al. Mechanism of rapid electron transfer during oxygen activation in the R2 subunit of *Escherichia coli* ribonucleotide reductase. 1. Evidence for a transient tryptophan radical. J. Am. Chem. Soc. 2000; 122:12195–12206.

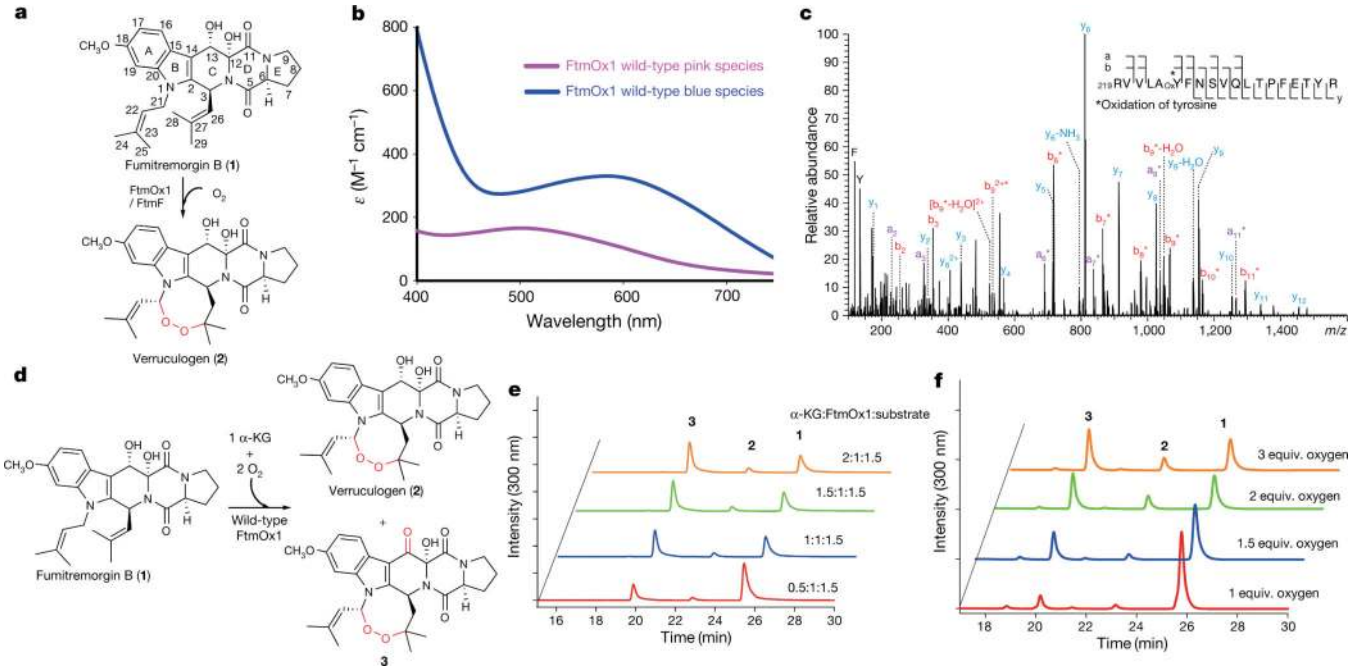

Figure 1. Enzymatic characterization of wild-type FtmOx1

a, Proposed FtmOx1 reaction. **b**, Formation of the FtmOx1-Fe^{II}–α -KG binary complex under anaerobic conditions (pink trace). Self-hydroxylation reaction upon exposure of the binary complex to O_2 (blue trace). **c**, Electrospray ionization MS/MS analysis of the blue species in **b** is consistent with the oxidation of Y224 to DOPA224. **d**, Products formed in the FtmOx1 reaction. **e**, α -KG stoichiometry analysis in FtmOx1 catalysis. High performance liquid chromatography (HPLC) chromatograms of FtmOx1 reactions with various amounts of α -KG. Identities of the peaks were assigned based on nuclear magnetic resonance (NMR) and high-resolution mass spectrometry (see Supplementary Information). **f**, O_2 stoichiometry analysis in FtmOx1 catalysis. HPLC chromatograms of FtmOx1 reactions contained fumitremorgin B (360 μ M), FtmOx1 (240 μ M), and α -KG (480 μ M) when variable amounts of oxygen-saturated buffer were added to initiate the reaction.

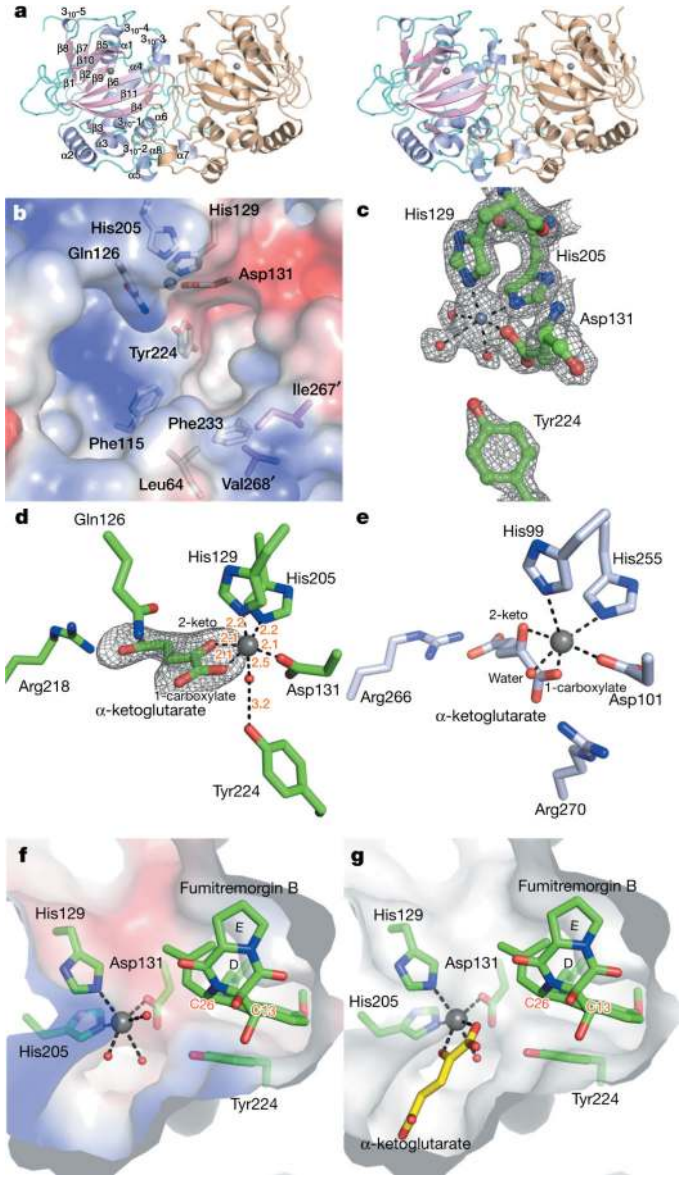

Figure 2. Structures of FtmOx1

a, Overall architecture of FtmOx1 shown as a functional dimer with one monomer colour-coded based on secondary structures (shown as stereo images). The iron centre is labelled as a grey sphere. **b**, FtmOx1 active site shown in the electrostatistic mode. **c**, FtmOx1 metallo-centre electron density ($2mF_o - DF_c$ map) at 1σ contour. The coordination of iron is represented by dashed lines. **d**, FtmOx1-Fe^{II}–α -KG binary complex. The α -KG molecule was modelled into a composite omit map ($mF_o - DF_c$ map) contoured to 2.8σ. The coordination of iron is represented by dashed lines with distances labelled (units, Å). **e**, α -KG binding mode of TauD (PBD accession code 1OS7). TauD is shown in an identical orientation relative to that of FtmOx1 in **d** to highlight their differences in active site topologies. **f**, Structure of the FtmOx1-Fe^{II}–fumitremorgin B complex. **g**, Superimposition of the binary structures of FtmOx1-Fe^{II}–α -KG and FtmOx1–fumitremorgin B. Y224 is highlighted in pink.

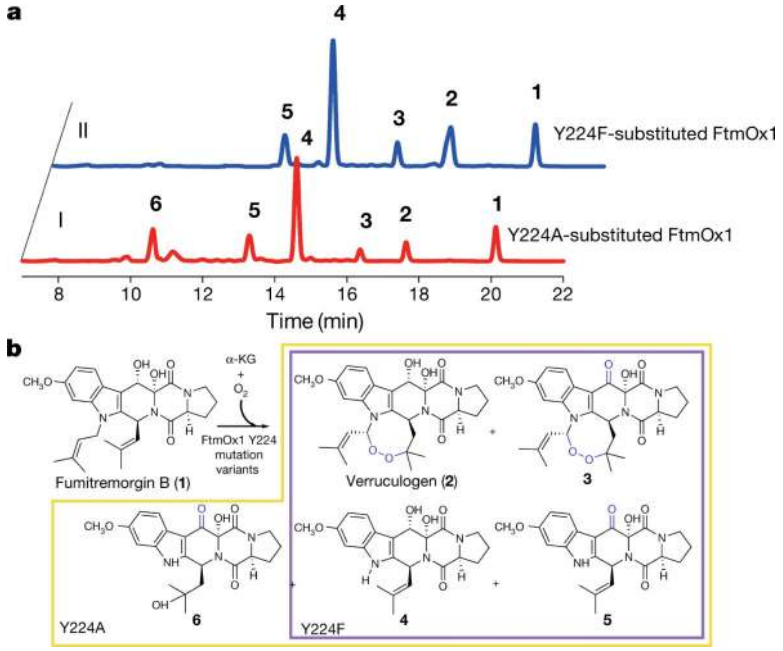

Figure 3. Characterization of Y224A- and Y224F-substituted FtmOx1

a, HPLC profiles of reactions from the two FtmOx1 variants, Y224A and Y224F. Both traces were conducted in reaction mixture containing FtmOx1 Y224 variants (240 μ M), fumitremorgin B (240 μ M), α -KG (720 μ M) and O_2 (480 μ M). Trace I, HPLC chromatograms of the reaction using Y224A-substituted FtmOx1; trace II, HPLC chromatograms of the reaction using Y224F-substituted FtmOx1. Note that a new column was used for the mutant analyses relative to the one in wild-type FtmOx1 characterizations, which led to the differences in retention times relative to the other HPLC traces. **b**, Products formed in reactions using either Y224F- or Y224A-substituted FtmOx1 variants. The compounds were characterized using NMR and MS (see Supplementary Information).

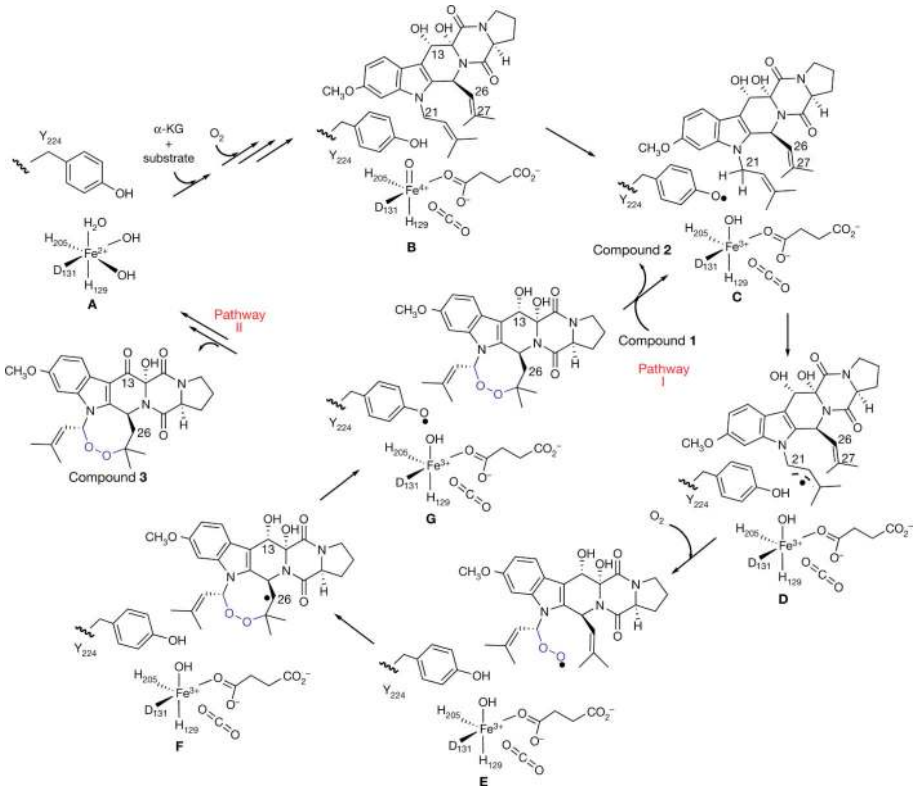

Figure 4. Proposed FtmOx1 mechanistic model

The oxygen–oxygen bonds shown in blue highlight the incorporation of endoperoxide into the substrate fumitremorgin B.

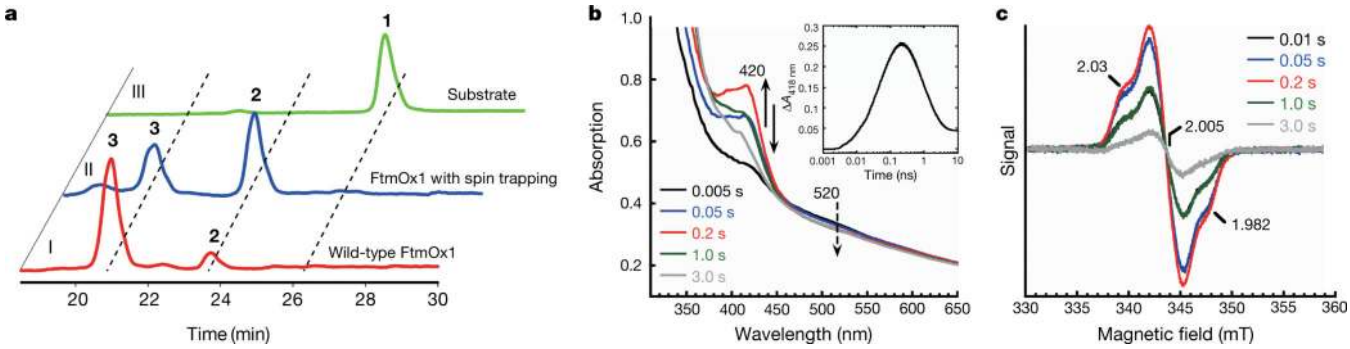

Figure 5. Evidence for transient radical species in the reaction pathway

a, HPLC chromatograms of FtmOx1 reaction under three different conditions. The reaction mixture contained FtmOx1 (240 μ M), fumitremorgin B (200 μ M), α -KG (300 μ M), and was initiated with O_2-saturated buffer. Trace I, FtmOx1 reaction; trace II, FtmOx1 reaction in the presence of 10 mM DMPO; trace III, FtmOx1 substrate alone. **b**, Absorbance changes upon mixing the O_2-saturated buffer with the reaction mixture in 100 mM Tris-HCl (pH 7.5) buffer containing FtmOx1 (0.65 mM), Fe^{II} (0.58 mM), fumitremorgin B (0.58 mM) and α -KG (12 mM). The decay of the Fe–α -KG complex charge transfer band centred at ~520 nm (dashed arrow) and the formation and decay of the spectral feature centred at ~420 nm (arrow) are highlighted. Inset: time-dependent absorbance change at 420 nm. The absorbance reported in **b** was obtained by blanking the spectrometer with the anaerobic buffer containing 100 mM Tris-HCl (pH 7.5). The absorbance reported in the inset was obtained by subtracting the absorbance at 420 nm of the 2 ms spectrum from all other spectra recorded. The trace is the average of two trials. **c**, Spectroscopic evidence for transient radical species. X-band EPR spectra measured at 19 K of reaction samples freeze-quenched at the indicated time points. Measurement conditions: microwave frequency, 9.64 GHz; microwave power, 2 μ W; modulation amplitude, 1 mT; and modulation frequency, 100 kHz.